NTNU

Norwegian University of
Science and Technology

Velocity ratio estimation using AVA attributes in VTI media

Arslan Zahid

Petroleum Geosciences
Submission date: June 2017
Supervisor: Kenneth Duffaut, IGP

Norwegian University of Science and Technology
Department of Geoscience and Petroleum

Abstract

Amplitude variation with angle (AVA) analysis is one of the fundamental tools for hydrocarbon detection and reservoir characterization. The background trend as a function of intercept against gradient for various $\langle Vp \rangle / \langle Vs \rangle$ ratios are well defined assuming isotropic media only. However, how the anisotropy changes this background trend is not being investigated. Therefore, this study shows the effects induced by anisotropy assuming VTI symmetry, on background trends, reflectivity by using the weak contrast two term approximation. Moreover, analytical expressions for the estimation of average *Vp* and *Vp/Vs* ratios from AVA attributes (*A* and *B*) are derived and then modelled using well and seismic data from Norwegian Sea for both the isotropic and VTI media respectively.

To accomplish this work, well log data, synthetic seismic CMP gathers and real seismic data were used to calculate the intercept-gradient ratios which were then implemented to generate the plots, background trends, modelling of average *Vp* and *Vp/Vs* ratios using the derived explicit equations. The modelled results obtained from the log data, synthetic seismic CMP gathers and real seismic data for the estimation of average *Vp* and *Vp/Vs* ratios are quite adequate, good. Some of the major problems encountered in this modelling was the instability caused by very low values of intercept-gradient ratios, resulting in very high values of estimated average *Vp* and *Vp/Vs* ratios, approaching infinity in magnitude. This complication was solved by applying the smoothing function. However, some of the original well data would get removed during the process of attaining the perfect modelling outcome, thereby, suggesting the need to find the optimal parameters of smoothing filter function. Another difficulty came across when modelling of estimated data values was the frequency bandwidth problem which was investigated as well. Likewise smoothing, this also requires the need to find the optimal frequency bandpass filter.

Acknowledgements

I would like to thank my supervisor Kenneth Duffaut for giving me many valuable, useful discussions and comments, and assisting me with the problems encountered in MATLAB and GEOVIEW (Hampson-Russel) regarding this work.

I thank Norwegian Petroleum Directorate (NPD) for the provision of well data.

I would like to thank CGG for permitting me the full license of GEOVIEW (Hampson-Russel) and NTNU for MATLAB's license as well.

Table of contents

List of figures vii

Nomenclature ix

1 Introduction 1

2 Theory 5

2.1 Background trend 5

2.2 Isotropic medium 5

2.2.1 Deriving an expression for an average Vs/Vp by using general intercept versus gradient equation in isotropic media 6

2.3 Anisotropic medium (VTI) 7

2.3.1 Deriving an expression for estimating average Vp in VTI media by using general intercept versus gradient equation 9

3 Methodology 11

3.1 Background trend 11

3.2 Plane-wave reflection coefficient versus angle of incidence in isotropic and VTI media 11

3.3 Well logs 11

3.4 Synthetic seismic CMP gather and AVA attributes using GEOVIEW 13

3.5 Seismic angle stacks 14

3.6 Estimating ⟨Vp⟩/⟨Vs⟩ from B/A using well and seismic data 14

3.7 Smoothing of the data 16

3.7.1 Smoothing A and B for estimating ⟨Vp⟩/⟨Vs⟩ 16

3.7.2 Smoothing B/A for estimating ⟨Vp⟩/⟨Vs⟩ 16

3.7.3 Smoothing ⟨Vp⟩/⟨Vs⟩ 17

4 Results 19

4.1 Background trends comparison 19

4.2 Plane-wave reflection coefficient as function of angle of incidence in isotropic and VTI media 19

4.3 Estimated average Vp/Vs from B/A using log based data 22

4.3.1 Estimating ⟨Vp⟩/⟨Vs⟩ from smoothing data B/A in isotropic media 22

4.3.2 Estimating ⟨Vp⟩/⟨Vs⟩ from smoothing data B/A in VTI media 23

4.3.3 Comparison of ⟨Vp⟩/⟨Vs⟩ ratios between isotropic and anisotropic (VTI) media using log based data 25
4.4 Estimated average Vp/Vs from B/A using synthetic seismogram 28
4.4.1 Comparison of ⟨Vp⟩/⟨Vs⟩ ratios between isotropic and anisotropic (VTI) media using synthetic seismogram 28
4.5 Estimated average Vp/Vs from B/A using real seismic data 30

5 Discussion 37
6 Conclusions 39
7 Future work 41
8 References 43
9 Bibliography 45

APPENDIX A: Empirical coefficients
APPENDIX B: Well logs using GEOVIEW
APPENDIX C: Instability problem
APPENDIX D: More smoothing results using log based well data

D.1 Estimating ⟨Vp⟩/⟨Vs⟩ from smoothing data A and B in isotropic media
D.2 Smoothing the estimated ⟨Vp⟩/⟨Vs⟩ data in isotropic media
D.3 Resampling of well logs to the resolution of synthetic data

APPENDIX E: More estimated results using seismic data
APPENDIX F: Seismic frequency bandwidth problem

List of figures

Figure 1. Conventional well logs and estimated anisotropic well logs produced using well 6608/10-3, Norne Field on MATLAB. 12
Figure 2. Conventional well logs and estimated anisotropic well logs produced using well 7121/4-1, Snøhvit Field on MATLAB. 13
Figure 3. Ricker Wavelet of 25 Hz frequency generated in GEOVIEW. 14
Figure 4. B/A versus $\langle Vp \rangle / \langle Vs \rangle$ for both isotropic and VTI media. 16
Figure 5. Intercept versus gradient comparison for isotropic and VTI media assuming a linear Vp versus Vs trend. 19
Figure 6. Plane-wave reflection coefficient versus the angle of incidence for isotropic and VTI media using the two-term approximation. 21
Figure 7. ⟨Vp⟩ and ⟨Vp⟩/⟨Vs⟩ estimated by smoothing the response data B/A in isotropic media. Well 6608/10-3, Norne Field. 22
Figure 8. ⟨Vp⟩ and ⟨Vp⟩/⟨Vs⟩ estimated by smoothing the response data B/A in isotropic media. Well 7121/4-1, Snøhvit Field. 23
Figure 9. ⟨Vp⟩ and ⟨Vp⟩/⟨Vs⟩ estimated by smoothing the response data B/A in a VTI media. Well 6608/10-3, Norne Field. 24
Figure 10. ⟨Vp⟩ and ⟨Vp⟩/⟨Vs⟩ estimated by smoothing the response data B/A in a VTI media. Well 7121/4-1, Snøhvit Field. 25
Figure 11. ⟨Vp⟩ and ⟨Vp⟩/⟨Vs⟩ estimated by smoothing the response data B/A using span of 2001 and constant m, g and c for isotropic and VTI media. Well 6608/10-3, Norne Field and Well 7121/4-1, Snøhvit Field. 27
Figure 12. ⟨Vp⟩ and ⟨Vp⟩/⟨Vs⟩ estimated by smoothing the response data B/A using span of 309 and constant m, g and c for isotropic and VTI media. Well 6608/10-3, Norne Field and Well 7121/4-1, Snøhvit Field. 29
Figure 13. ⟨Vp⟩ and ⟨Vp⟩/⟨Vs⟩ estimated by smoothing the seismic response data B/A for VTI media, Norne Field. 30
Figure 14. Intercept and gradient cross section for estimation of ⟨Vp⟩ and ⟨Vp⟩/⟨Vs⟩ ratios across the whole 2D seismic line. 32
Figure 15. Estimated B/A cross section for modelling of ⟨Vp⟩ and ⟨Vp⟩/⟨Vs⟩ ratios across the whole 2D seismic line. 33
Figure 16. Estimated ⟨Vp⟩ and ⟨Vp⟩/⟨Vs⟩ cross sections of the seismic response data B/A for VTI media, Norne Field. 34

Nomenclature

A	AVO Intercept
AVA	Amplitude Versus Angle
AVO	Amplitude Versus Offset
B	AVO Gradient
C	AVO Curvature
c	Intercept
CMP	Common Mid-Point
d	Coefficient of Gardner et al. (1974) density-velocity equation
g	Coefficient of Gardner et al. (1974) density-velocity equation
m	Slope
P-wave	Primary wave
Rp	Reflection coefficient of P-wave
sh	Shale
sst	Sandstone
S-wave	Secondary wave
V_{clay}	Volume of clay in fraction
Vp	Velocity of P-wave
$\langle Vp \rangle$	Average P-wave velocity
$V_{P\ quartz}$	P-wave velocity of quartz
$V_{P\ water}$	P-wave velocity in water
Vs	Velocity of S-wave
$\langle Vs \rangle$	Average S-wave velocity
V_{SH}	Horizontal S-wave velocity
V_{sh}	Volume of shale in fraction
VTI	Vertical Transverse Isotropy
γ	Thomsen Gamma parameter
δ	Thomsen Delta parameter
ε	Thomsen Epsilon parameter
θ	Incidence angle
ρ	Density

1 Introduction

Amplitude variation with angle (AVA) or offset (AVO) analysis has turned out to be a successful tool for detection of hydrocarbon reservoirs and to do a better correlation between seismic and well data. Seismic AVO crossplotting using Biot-Gassmann equations gives the basis for understanding the effects of fluid substitution on AVO attributes, Ross (2000). Ostrander (1984) showed that the Poisson's ratio has a major impact on changes in reflection coefficient as a function of incidence angle and variation of seismic reflection amplitude against angle of incidence can act as direct hydrocarbon indicators. AVO analysis today implies both weak contrast and small angles approximations.

According to Castagna et al. (1998), the AVO intercept (*A*) and gradient (*B*) forms a well-defined background trend when crossplotted, for example, shales and brine saturated sandstones and is related to the average *Vp/Vs* ratio of the rocks. As the average *Vp/Vs* ratio increases, the slope of the background trend rotates counter clockwise. Furthermore, any deviation from the background trend can be due to presence of hydrocarbons or lithologies with anomalous elastic properties. The reflection coefficient variation against the incident angle is given by Zoeppritz (1919) equations. Castagna et al. (1998) used Aki and Richards (1980) weak contrast approximation and proposed the P-wave reflection coefficient as a function of angle of incidence (θ) by the equation:

$$Rp\,(\theta) = A + B\,sin^2(\theta) + C\,sin^2(\theta)\,tan^2(\theta) \tag{1}$$

where *Rp* is the reflection coefficient as a function of angle of incidence (θ) with

$$A = \frac{1}{2}\left(\frac{\Delta Vp}{\langle Vp\rangle} + \frac{\Delta\rho}{\langle\rho\rangle}\right); \tag{2}$$

$$B = \frac{1}{2}\,\frac{\Delta Vp}{\langle Vp\rangle} - 2\left(\frac{\langle Vs\rangle}{\langle Vp\rangle}\right)^2\left(2\frac{\Delta Vs}{\langle Vs\rangle} + \frac{\Delta\rho}{\langle\rho\rangle}\right); \tag{3}$$

$$C = \frac{1}{2}\,\frac{\Delta Vp}{\langle Vp\rangle}; \tag{4}$$

where $\langle Vp\rangle$, $\langle Vs\rangle$ and $\langle\rho\rangle$ represents the average P-wave velocity, S-wave and density across the interface, respectively. Similarly, ΔVp represents the change in P-wave velocity, ΔVs is the change in S-wave velocity and $\Delta\rho$ is the change in density across the interface, correspondingly.

Anisotropy plays a vital role for computing or governing properties particularly for hydrocarbon detection, exploration, reservoir characterization, since in the field, outcrop, properties of rocks are generally anisotropic rather than being simply isotropic. Rock

anisotropy can be described, quantified by the anisotropic parameters epsilon *'ε'*, gamma *'γ'* and delta *'δ'* as given by Thomsen (1986).

Leaney (1993) measured the anisotropy using Walkaway surveys and showed its importance on AVO using anisotropic AVO Synthetics which may cause wrong interpretations of AVO anomalies. Likewise, Transverse isotropy can alter the traditional AVO analysis as showed by Wright (1987), Banik (1987), Kim et al. (1993), Thomsen (1993) and Rüger (1997). Similarly, Alkhalifah and Rampton (2001) exhibited that the anisotropy could be used to distinguish between shales and sands in the subsurface; lithology interpretation. Li and Pickford (2002) showed that the anisotropic rock properties are important for seismic analysis using anisotropic synthetic seismogram and anisotropic AVO extraction and inversion. Johnston and Christensen (1995) found out that the variation in seismic velocity caused by anisotropy is proportional to the clay content, orientation index. Wang (2001) demonstrated that the shales are seismically anisotropic and concluded that the anisotropic effects for far offset seismic processing and interpretation results in significantly warped seismic images and false AVO results if isotropy is assumed. Also, anisotropy is further enhanced by increase in compaction, consolidation as clay minerals tend to align themselves in the direction perpendicular to overburden pressure; resulting in increased seismic velocity in the direction of bedding as showed by Li (2006).

Castagna et al. (1998) presented a framework for AVO gradient and intercept analysis using different relationships for various background trend cases. However, all the work was done assuming isotropic media. In this work, I would investigate the effects of anisotropy on the background trend and would see how the anisotropic plots differ when compared to isotropic case. The next step involves the AVA attributes, i.e., intercept and gradient, and how they can be used to estimate average *Vp* and *Vp/Vs* ratio in anisotropic, VTI media. For simplicity, I would be using the two term Aki and Richards (1980) weak contrast approximation for calculating the reflection coefficient as a function of the average angle of incidence ($0° < \theta < 40°$) in a VTI media given below

$$Rp\,(\theta) = A + B' \sin^2(\theta) \tag{5}$$

where *A* is given by equation (2),

$$B' = \frac{1}{2}\frac{\Delta Vp}{\langle Vp\rangle} - 2\left(\frac{\langle Vs\rangle}{\langle Vp\rangle}\right)^2\left(2\frac{\Delta Vs}{\langle Vs\rangle} + \frac{\Delta\rho}{\langle\rho\rangle}\right) + \frac{\Delta\delta}{2}, \tag{6}$$

and $\Delta\delta$ represents the contrast in delta values of upper layer and lower layer across the interface, Thomsen (1993).

This two term approximation is generally accredited to Shuey (1985), making the calculations simple by linearizing the expression. For the anisotropy, the parameters and relationships would be used from Thomsen (1986) and Li (2006). The anisotropy model is chosen as vertical transverse isotropy (VTI) as discussed by Rüger (1997) and it is associated with shale and layering and is one of the common type of anisotropy found in the outcrop.

Deriving the general intercept versus gradient equation for estimating average *Vp* as a function of '*g*', clay content, '*m*' and '*c*'; for the linear *Vp* versus *Vs* background trend case is a key factor for this study. By using this derived equation, explicit expressions would be derived as well to estimate average *Vp* and *Vp/Vs* ratios in isotropic and VTI media. The well data from the Norwegian Sea (Norne and Snøhvit) including logs (P-wave & S-wave velocities, density, volume of shale) would be used to evaluate anisotropic parameters delta and epsilon; reflectivity modelling using equation (5), conventional and anisotropic well logs, synthetic seismic CMP gathers, computing AVA attributes and eventually estimating average *Vp* and *Vp/Vs* ratios. In addition to well data, real seismic data, i.e., angle stacks (Near, Mid and Far) would also be applied for the estimation of average *Vp* and *Vp/Vs* ratios to see the comparison with the log based data and synthetic seismogram. At the end, an answer would be given to the question that is it possible to estimate average *Vp* and *Vp/Vs* ratios from AVA attributes? All of the above tasks would be done by using the software MATLAB and GEOVIEW (Hampson-Russell).

2 Theory

2.1 Background trend

The background trend is a function of intercept against gradient which are related to elastic velocities and density, shown in equations (2) and (3). Gardner et al. (1974) developed a relationship between density and the velocity by the following equation

$$\rho = dVp^{g}. \tag{7}$$

If we take the derivative of this equation, assuming $\rho = \langle\rho\rangle$, we would get the expression

$$\frac{\Delta\rho}{\langle\rho\rangle} \sim g\frac{\Delta Vp}{\langle Vp\rangle}, \tag{8}$$

as showed by Castagna et al. (1998). Castagna et al. (1985) showed that for a linear *Vp* versus *Vs* relationship, assuming $Vp = \langle Vp\rangle$ and $Vs = \langle Vs\rangle$, we have the equation:

$$\langle Vp\rangle = m\,\langle Vs\rangle + c \tag{9}$$

where m and c are empirical coefficients.

If we combine these equations from (2) to (8), we would get a general relationship between intercept and gradient for both isotropic and anisotropic (VTI) media. Typical values of *m*, *c*, *d* and *g* for different lithologies are given in Appendix A.

2.2 Isotropic medium

Isotropy is the nature of a media having identical, uniform properties in all directions of the media. General intercept versus gradient equation for isotropic media can be derived by using equation (2) and inserting equation (8) in it, it can be re-arranged in the form as

$$\frac{\Delta Vp}{\langle Vp\rangle} = \frac{2A}{(1+g)}. \tag{10}$$

Similarly, equation (9) can be re-arranged as

$$\langle Vs\rangle = \frac{1}{m}\langle Vp\rangle - \frac{1}{m}c; \tag{11}$$

taking derivative of it with respect to $\langle Vs\rangle$ and doing further simplification, it can be expressed as

$$\frac{\Delta Vs}{\langle Vs\rangle} = \frac{\Delta Vp}{m\,\langle Vs\rangle}. \tag{12}$$

Now using equation (3) and inserting the equations (8) and (12) in it, we would get the expression as

$$B = \frac{\Delta Vp}{\langle Vp \rangle}\left[\frac{1}{2} - 2\left(\frac{\langle Vs \rangle}{\langle Vp \rangle}\right)^2\left(2\frac{\langle Vp \rangle}{m\langle Vs \rangle} + g\right)\right]. \quad (13)$$

Finally, combining equations (10) and (13), a general equation in the *A*-*B* plane for the background reflections assuming isotropic media is obtained as showed by Castagna et al. (1998), given below

$$B = \frac{A}{1+g}\left[1 - 4\frac{\langle Vs \rangle}{\langle Vp \rangle}\left(\frac{2}{m} + g\frac{\langle Vs \rangle}{\langle Vp \rangle}\right)\right]. \quad (14)$$

Substituting equation (9) into equation (14) yields

$$B = \frac{A}{1+g}\left[1 - 4\frac{\langle Vp \rangle - c}{m\langle Vp \rangle}\left(\frac{2}{m} + g\frac{\langle Vp \rangle - c}{m\langle Vp \rangle}\right)\right] \quad (15)$$

which is an intercept versus gradient equation for a linear *Vp* versus *Vs* background trend case as a function of 'g', '*m*' and *'c'*. As showed by Gardner et al. (1974), the value of 'g' is equal to 1/4 for most sedimentary rocks. If we put this value of *'g'* in equation (15), we would get

$$B = \frac{4}{5}A\left[1 - \frac{1}{(m\langle Vp \rangle)^2}(\langle Vp \rangle - c)(9\langle Vp \rangle - c)\right]. \quad (16)$$

Similarly, substituting equation (9) into equation (2) and using 1/4 as a value of *'g'*, we would get

$$A = \frac{5}{8}\frac{\Delta Vp}{\langle Vp \rangle}. \quad (17)$$

Both the equations (16) and (17) are the same equations as showed by Castagna et al. (1998) which verifies the validity of equation (15) for isotropic media. For the VTI media, we just add the anisotropic parameter delta in the gradient term to get the expressions for VTI anisotropy as shown in equation (6).

2.2.1 Deriving an expression for an average *Vs/Vp* by using general intercept versus gradient equation in isotropic media

By using equation (14) and further simplifying it, the expression can be re-arranged in the form as

$$B = \frac{A}{1+g}\left[1 - \frac{8}{m}\frac{\langle Vs \rangle}{\langle Vp \rangle} - 4g\left(\frac{\langle Vs \rangle}{\langle Vp \rangle}\right)^2\right], \quad (18)$$

$$(1+g)\frac{B}{A} = 1 - \frac{8}{m}\frac{\langle Vs \rangle}{\langle Vp \rangle} - 4g\left(\frac{\langle Vs \rangle}{\langle Vp \rangle}\right)^2, \quad (19)$$

$$4g\left(\frac{\langle Vs \rangle}{\langle Vp \rangle}\right)^2 + \frac{8}{m}\frac{\langle Vs \rangle}{\langle Vp \rangle} + \left(\frac{B}{A}(1+g) - 1\right) = 0. \quad (20)$$

Now the above equation is being expressed in the form of quadratic equation $ax^2 + bx + c = 0$ which can now be solved by using the quadratic formula

$$x = \frac{-b \pm \sqrt{b^2 - 4ac}}{2a}. \tag{21}$$

So, by using the equation above with $a = 4g$, $b = 8/m$ and $c = \left(\frac{B}{A}(1+g) - 1\right)$,

$$x = \frac{\langle Vs \rangle}{\langle Vp \rangle} = \frac{-\frac{8}{m} + \sqrt{\left(\frac{8}{m}\right)^2 - (16g)\left(\frac{B}{A} + g\frac{B}{A} - 1\right)}}{8g}. \tag{22}$$

From the above expression, we are supposed to get two solutions of *x* due to the square root term. However, we would only use the positive values from this term since we know that the ratio $\langle Vs \rangle / \langle Vp \rangle$ can't be negative. By taking the inverse of expression (22), we can get the desired values for $\langle Vp \rangle / \langle Vs \rangle$ and by using equation (9), $\langle Vp \rangle$ can be estimated as well in an isotropic media.

2.3 Anisotropic medium (VTI)

Unlike isotropy, anisotropy is the property of a media having different properties in different directions, i.e., directionally dependent. Seismic Anisotropy can be defined as the dependence of velocity on direction or upon angle, Thomsen (2002). The seismic anisotropy is usually referred to as transverse isotropy because there is isotropy in the horizontal or vertical plane.

The anisotropy parameters of the rock are given by Thomsen (1986) as

$$\varepsilon = \frac{C_{11} - C_{33}}{2C_{33}},$$

$$\gamma = \frac{C_{66} - C_{44}}{2C_{44}},$$

$$\delta = \frac{(C_{13} + C_{44})^2 - (C_{33} - C_{44})^2}{2C_{33}(C_{33} - C_{44})}$$

where C_{11}, C_{13}, C_{33}, C_{44} and C_{66} are the elastic coefficients in a transverse isotropy.

Thomsen (1993) simplified these parameters for weak anisotropy to

$$\varepsilon \approx \frac{V_P(90°) - V_{po}}{V_{po}},$$

$$\gamma \approx \frac{V_{SH}(90°) - V_{so}}{V_{so}},$$

$$\delta \approx 4\left[\frac{V_p(45°)}{V_p(0°)} - 1\right] - \left[\frac{V_p(90°)}{V_p(0°)} - 1\right]$$

with

$$V_{po} = \sqrt{\frac{C_{33}}{\rho}},$$

$$V_{so} = \sqrt{\frac{C_{44}}{\rho}},$$

where $V_{SH}(90°)$ is the horizontal S-wave velocity, V_{po} and V_{so} are the vertical P-wave and S-wave velocities, respectively.

Since we are interested in epsilon *'ε'* and delta *'δ'* only, assuming VTI anisotropy, (Li, 2006) developed a relationship between epsilon and delta by the expression;

$$\delta = 0.32\,\varepsilon \tag{23}$$

and epsilon is given by the expression;

$$\varepsilon = \frac{0.60 * V_{clay} * (V_P - V_{P\,water})}{V_{P\,quartz} - V_{P\,water} - 2.65 * V_{clay}} \tag{24}$$

where

0.60 is the P-wave anisotropic parameter for clay, V_{clay}= Volume of clay, $V_P = V_{po}$, $V_{P\,water}$ = approximate P-wave velocity in water and $V_{P\,quartz}$ = P-wave velocity of quartz, which would be used in this treatise. According to (Li, 2006), the anisotropy parameters increase linearly with V_{po} or V_{so} for a given clay volume, and the greater the clay content, the greater the increase. Increase in clay content in tight rocks tends to change isotropic rocks to anisotropic rocks with maximum anisotropy at clay mineral point (zero porosity clay point).

Another relationship for delta *'δ'* which could be considered is given by (Ryan-Grigor, 1997) in terms of *Vp/Vs* and C_{13}/C_{44} as

$$\delta = \frac{\left[1 + \left(\frac{C_{13}}{C_{44}}\right)\right]^2 - \left[\left(\frac{V_p}{V_s}\right)^2 - 1\right]^2}{2\left(\frac{V_p}{V_s}\right)^2\left[\left(\frac{V_p}{V_s}\right)^2 - 1\right]^2} \tag{25}$$

where

$$\frac{C_{13}}{C_{44}} = 3.61\frac{V_p}{V_s} - 5.06. \tag{26}$$

As mentioned in previous chapter, the reflection coefficient for P-wave as a function of incident angle (θ) is given by equation (1) for isotropic media and equation (5) for anisotropic media. We can see that the first term '*A*', given by equation (2), is free from any anisotropy parameter in both equations (1) and (5) which clearly shows that anisotropy is present only for the second term '*B*'. Since '*C*' is going to be neglected as the two-term approximation would be used in

this study, therefore, equation (23) would be applied and the parameters for this relationship would be considered from (Li, 2006).

For the VTI media, the anisotropy is resulted due to the delta in the gradient term as shown in equation (6). The delta is related to epsilon by the expression (23). By using equation (24), delta can be expressed as

$$\frac{\delta}{0.32} = \frac{0.60 * V_{clay} * (V_P - V_{P\,water})}{V_{P\,quartz} - V_{P\,water} - 2.65 * V_{clay}}. \tag{27}$$

If we take derivative of the above equation with respect to V_P and divide it by 2, the final expression becomes

$$\frac{\Delta\delta}{2} = \frac{0.192 * V_{clay} * \Delta V_P}{2\,(V_{P\,quartz} - V_{P\,water} - 2.65 * V_{clay})}. \tag{28}$$

Now by using ΔV_P from equation (10), the above become expression is expressed in terms of *A* and average *Vp*

$$\frac{\Delta\delta}{2} = \frac{0.192 * V_{clay} * \langle Vp\rangle * A}{(V_{P\,quartz} - V_{P\,water} - 2.65 * V_{clay}\,)\,(1+g)}. \tag{29}$$

Equation (15) shows the general intercept versus gradient equation as a function of 'g', 'm' and *'c'* in isotropic media for a linear *Vp* versus *Vs* background trend case. This equation can further be simplified as

$$B = \frac{A}{1+g}\left[1 - \frac{4}{(m\,\langle Vp\rangle)^2}(\langle Vp\rangle - c)(2\,\langle Vp\rangle + g\,(\langle Vp\rangle - c))\right]. \tag{30}$$

For VTI media, we would add the anisotropic parameter 'delta' in it using equation (29) and obtain the expression as

$$\begin{aligned} B = \frac{A}{1+g}\left[1 - \frac{4}{(m\,\langle Vp\rangle)^2}(\langle Vp\rangle - c)(2\,\langle Vp\rangle + g\,(\langle Vp\rangle - c))\right] \\ + \left[\frac{0.192 * V_{clay} * \langle Vp\rangle * A}{(V_{P\,quartz} - V_{P\,water} - 2.65 * V_{clay}\,)(1+g)}\right] \end{aligned} \tag{31}$$

which is the general intercept versus gradient equation as a function of 'g', 'm' and *'c'* in VTI media for a linear *Vp* versus *Vs* background trend case.

2.3.1 Deriving an expression for estimating average *Vp* in VTI media by using general intercept versus gradient equation

By using equation (31) and simplifying it furthermore, it can be expressed as

$$\left(\frac{B}{A}(1+g)-1\right) = -\frac{4}{(m\,\langle Vp\rangle)^2}[2\,\langle Vp\rangle^2 + g\,\langle Vp\rangle\,(\langle Vp\rangle - c) - 2\langle Vp\rangle\,c - g\,c(\langle Vp\rangle - c)] + \frac{0.192 * V_{clay} * \langle Vp\rangle}{(V_{P\,quartz} - V_{P\,water} - 2.65 * V_{clay})}, \quad (32)$$

$$\left(\frac{B}{A}(1+g)-1\right)\langle Vp\rangle^2 = -\frac{4}{m^2}[2\,\langle Vp\rangle^2 + g\,\langle Vp\rangle^2 - gc\langle Vp\rangle - 2c\langle Vp\rangle - gc\langle Vp\rangle + gc^2] + \frac{0.192 * V_{clay} * \langle Vp\rangle^3}{(V_{P\,quartz} - V_{P\,water} - 2.65 * V_{clay})}, \quad (33)$$

$$\left[\frac{0.192 * V_{clay} * m^{\,2}}{(V_{P\,quartz} - V_{P\,water} - 2.65 * V_{clay})4}\right]\langle \boldsymbol{Vp}\rangle^3 + \left[-\frac{4}{m^2}\left(\frac{B}{A}(1+g)-1\right) - 2 - g\right]\langle \boldsymbol{Vp}\rangle^2 + [2gc + 2c]\langle \boldsymbol{Vp}\rangle - gc^2 = 0. \quad (34)$$

The above equation is being expressed in the form of cubic equation $ax^3 + bx^2 + cx + d = 0$ where

$$a = \left[\frac{0.192 * V_{clay} * m^{\,2}}{(V_{P\,quartz} - V_{P\,water} - 2.65 * V_{clay})4}\right],$$

$$b = \left[-\frac{4}{m^2}\left(\frac{B}{A}(1+g)-1\right) - 2 - g\right],$$

$$c = [2gc + 2c],$$

$$d = -gc^2$$

and $x = \langle Vp\rangle$. This cubic equation can now be solved algebraically, trigonometrically, or numerical approximations of the roots using root-finding algorithms. Since it's a third order degree equation, it would either have one real root, two real roots or three real roots. However, we would only be interested in the roots which are positive and lie in the range as of the well data values of *Vp*. By using equation (9), $\langle Vp\rangle/\langle Vs\rangle$ ratios can now be estimated as well.

3 Methodology

3.1 Background trend

Starting with the background trends, equations (16) and (17) would be used to make the *B/A* crossplot for isotropic material in MATLAB. The parameters, for example, $\langle Vp \rangle$ and $\langle Vp \rangle / \langle Vs \rangle$ for both equations are going to be taken from Castagna et al. (1998). For values of ΔVp, the MATLAB function 'linspace' would be used since its data is not given in the article.

Similarly, for anisotropic (VTI) material, the same MATLAB code and parameters would be applied but with the addition of anisotropy parameter 'delta' (δ) using equation (23). The value of delta regarding equation (23) is calculated by using equation (29).

The purpose for choosing VTI anisotropy in this study is because the clastic sediments, for example shale, has intrinsic, vertical transverse isotropic (VTI) properties and the earth is usually assumed as purely VTI when doing the global inversions for a 1-D anisotropy (Cobden et al., 2015).

3.2 Plane-wave reflection coefficient versus angle of incidence in isotropic and VTI media

Using model parameters for brine sand from Castagna et al. (1998) and angle of incidence ranging from 0° to 40°, a plot between reflection coefficient and incident angle would be generated for isotropic media. Relationships (2) and (3) for two term Aki and Richards (1980) weak contrast approximation are going to be used for this purpose. For anisotropic (VTI) media, the same model parameters would be applied but now equation (6) would be used instead of equation (3).

Likewise, using the model parameters from Rüger (1997) and the same angle of incidence as before, a plot between reflection coefficient and incident angle would be made for both isotropic and anisotropic media.

3.3 Well logs

The well data which is going to be used in this thesis is of the well 6608/10-3, Norne Field and well 7121/4-1, Snøhvit Field. The data is then loaded in the MATLAB which contains the information for true vertical depth, P-wave velocity, S-wave velocity (synthetic), density, volume of shale (clay content) and porosity. The anisotropy parameters epsilon 'ε 'and delta 'δ' are calculated by using the expression (23) and its subsequent model parameters from Li (2006), i.e., $V_{P\ water}$ = 1.5 km/s and $V_{P\ quartz}$ = 6.05 km/s.

Figure 1 and Figure 2 shows different logs produced by using the Norne and Snøhvit wells data. Formations tops are marked on the plots as well.

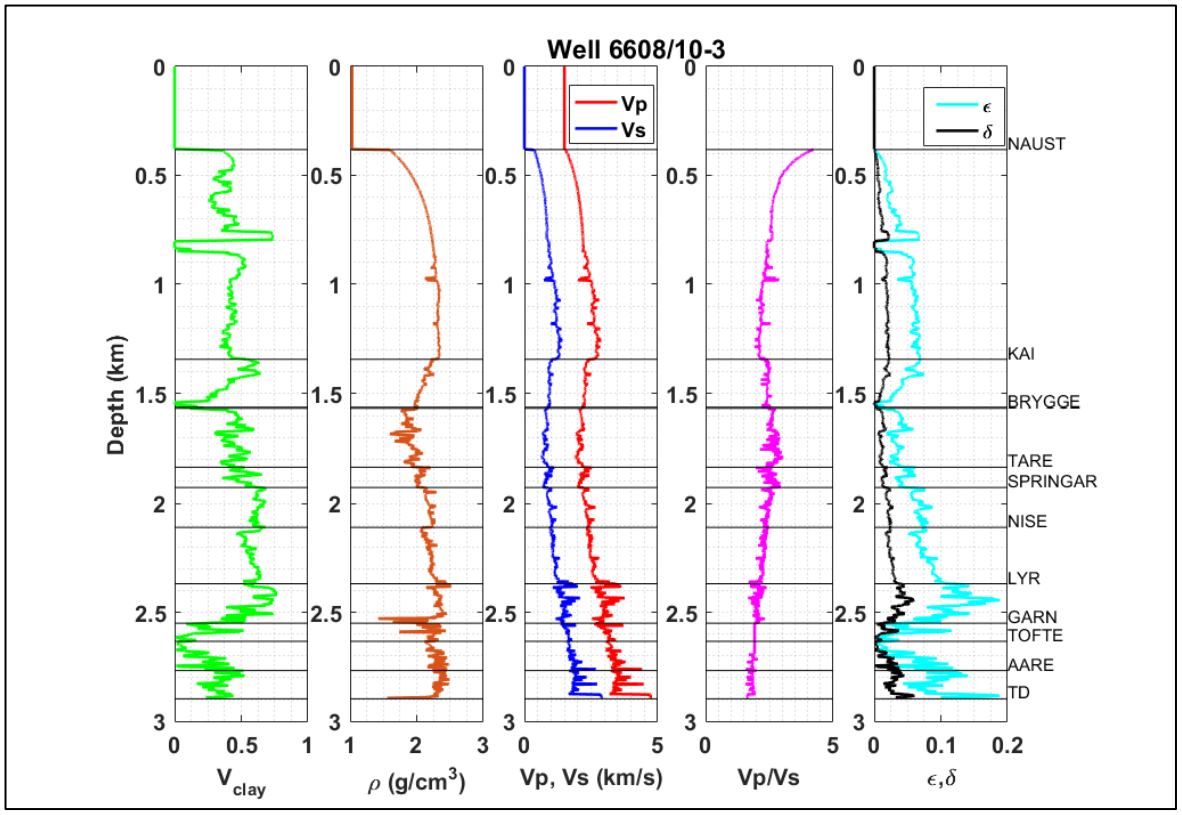

Figure 1. Conventional well logs and estimated anisotropic well logs produced using well 6608/10-3, Norne Field on MATLAB.

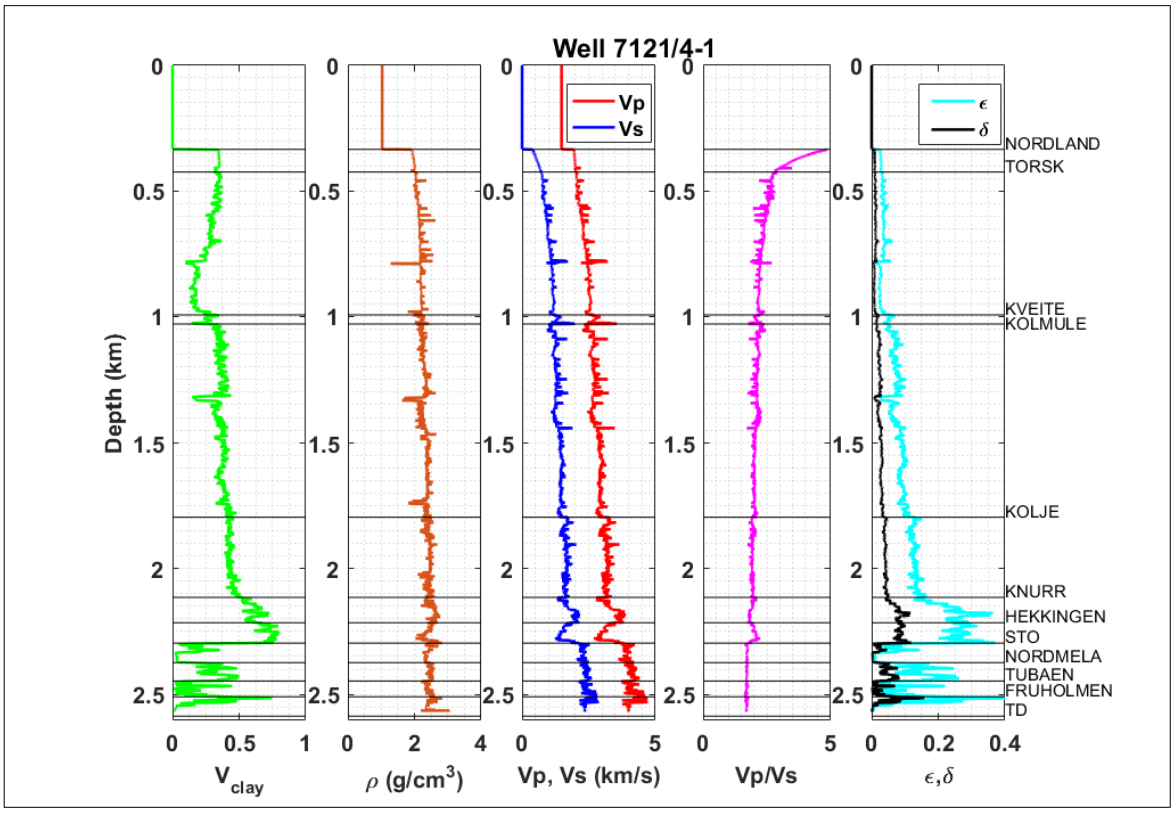

Figure 2. Conventional well logs and estimated anisotropic well logs produced using well 7121/4-1, Snøhvit Field on MATLAB.

Similarly, like MATLAB, the well data is loaded into the software 'GEOVIEW' with the inclusion of anisotropic data (δ, ε) calculated by using expression (23). This data is then again used to generate the well logs (conventional and anisotropic) and synthetic seismic CMP gather as shown in Appendix B.

3.4 Synthetic seismic CMP gather and AVA attributes using GEOVIEW

The 'AVO Analysis' in GEOVIEW for the extraction of intercept and gradient values requires 'AVO Modelling' which in turn requires creation of synthetic seismic CMP gather. The synthetic seismic CMP gather is thus produced by applying Ricker wavelet of 25 Hz frequency, normal polarity and angle of incidence ranging from 0° to 40°. This frequency is preferred because seismic data of depth around 3000 m is often recorded with this average frequency.

By using the function 'AVO Attribute Volume', *A* and *B* are generated for both the isotropic and VTI media and then exported to MATLAB to estimate $\langle Vp \rangle$ and $\langle Vp \rangle / \langle Vs \rangle$ ratios by using these data values. Figure 3 shows the wavelet used to generate synthetic seismic CMP gather.

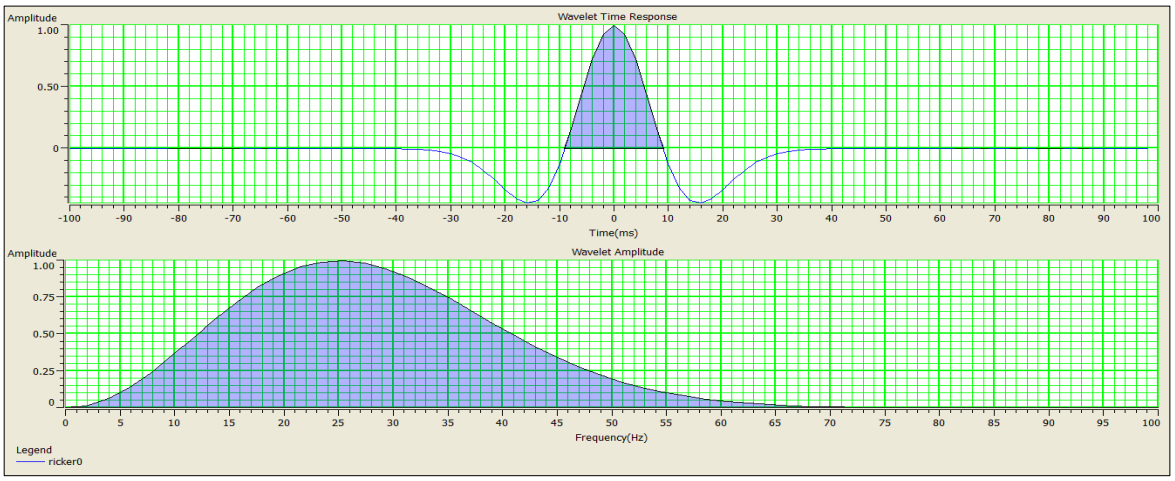

Figure 3. Ricker Wavelet of 25 Hz frequency generated in GEOVIEW.

3.5 Seismic angle stacks

The real seismic data of Norne Field, CMP angle gathers with 3 folds is used to produce Near, Mid and Far angle stacks. These angle stacks are then used to produce stack sections of intercept and gradient. These intercept and gradient stacks are then loaded in GEOVIEW where both *A* and *B* across the whole section are exported to MATLAB for estimating the average *Vp* and *Vp/Vs* ratios using the cubic equation (34) with constant mean values of *m*, *g* and *c* in a VTI media. The checkshot data of well 6608/10-3 was also used to do the time-depth conversion for estimating the desired results.

3.6 Estimating ⟨*Vp*⟩/⟨*Vs*⟩ from *B/A* using well and seismic data

As mentioned before, the average *Vp* and *Vp/Vs* ratios would be calculated by taking the inverse of equation (22) i.e., quadratic formula in isotropic media, and using cubic equation (34), explicitly derived for VTI media. In MATLAB, *A* and *B* are calculated from well log data by using their subsequent equations for isotropic and VTI media respectively. However, in GEOVIEW, these values are generated by doing the 'AVO Analysis' using the two term Aki and Richards (1980) weak contrast approximation, generating synthetic seismogram. These values are then exported to MATLAB for the estimation of ⟨*Vp*⟩ and ⟨*Vp*⟩/⟨*Vs*⟩ ratios. For real seismic data, as stated before, the intercept and gradient stacks would be used to produce *B/A* section across the whole 2D seismic line for estimation of ⟨*Vp*⟩ and ⟨*Vp*⟩/⟨*Vs*⟩ ratios.

Furthermore, we also know that the expressions for ⟨*Vp*⟩ and ⟨*Vp*⟩/⟨*Vs*⟩ ratios are dependent on *m*, *g* and *c* as well. Therefore, the values of *m*, *g* and *c* are going to be calculated in relation to

the formations, lithologies present in the well and thus by using the relationships given by Castagna et al. (1985) and Han (1986) for sandstones with clay content, referred to by Mavko et al. (2009), shown in Appendix A. The value of g according to equation (7), Gardner et al. (1974) is equal to 0.265 for shale and 0.261 for sandstone. Therefore, for shaly sandstone lithology, g can be computed by assuming the following relationship

$$g = (1 - V_{sh}) * g_{sst} + V_{sh} * g_{sh}, \tag{35}$$

where V_{sh} represents volume of shale (clay content), g_{sst} and g_{sh} are values of g for sandstone and shale correspondingly. Likewise, *m* and *c* are computed by assuming

$$m = (1 - V_{sh}) * m_{sst} + V_{sh} * m_{sh}, \tag{36}$$

$$c = (1 - V_{sh}) * c_{sst} + V_{sh} * c_{sh}, \tag{37}$$

where m_{sst}, m_{sh}, c_{sst} and c_{sh} are values of *m* and *c* for sandstone and shale respectively.

The other criteria for the values of *m*, *g* and *c* could be taken by using their mean values in proportion to the clay content i.e., 50%, of the well data. Furthermore, if we put *B/A* equals to zero in equation (22) then the relationship would be completely dependent on the values of *m* and *g*. Therefore, there would be some values of *m* and *g* which create instability problem as the $\langle Vp \rangle / \langle Vs \rangle$ would then be approaching the infinity values. See Appendix C for further details regarding this instability.

One important factor should be kept remember for estimation of $\langle Vp \rangle / \langle Vs \rangle$ that the values of *B/A* should not be positive for small ratios of $\langle Vp \rangle / \langle Vs \rangle$ as it would contradict directly with the results of Castagna et al. (1998) for *B/A* versus $\langle Vp \rangle / \langle Vs \rangle$ as shown in Figure 4. Exception is only at very high ratios of $\langle Vp \rangle / \langle Vs \rangle$ for which *B/A* becomes positive.

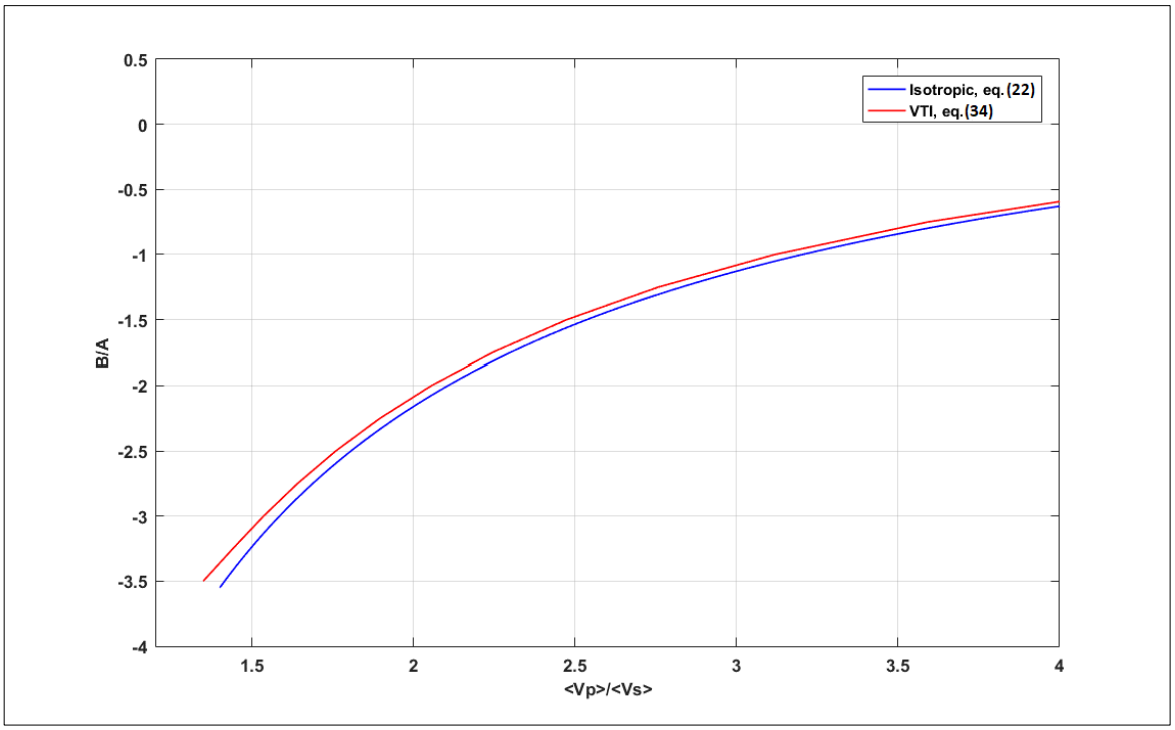

Figure 4. *B/A* versus $\langle Vp \rangle / \langle Vs \rangle$ for both isotropic and VTI media using linear (mudrock) *Vp* versus *Vs* and Gardner density (g = 1/4). Reproduced, Castagna et al. (1998).

3.7 Smoothing of the data

To accomplish the task of estimating $\langle Vp \rangle$ and $\langle Vp \rangle / \langle Vs \rangle$ ratios, various smoothing conditions would be applied to the response data to achieve the desired results. The purpose of using this function is to stabilize the model by filtering the data which causes instability, referred to Appendix C. The smoothing cases reviewed in this work are the following.

3.7.1 Smoothing *A* and *B* for estimating $\langle Vp \rangle / \langle Vs \rangle$

In this case, only the values of *A* and *B* are smoothed, filtered with span values of 2001, and 'rlowess', linearized method using the smooth function in MATLAB. The method 'rlowess' allocates lower weight to the outliers in the regression, set zero weight to data outside six mean absolute deviations, according to MATLAB. The smoothed data is then used to calculate the ratio *B/A* and thus, eventually computing $\langle Vp \rangle$ and $\langle Vp \rangle / \langle Vs \rangle$ ratios.

3.7.2 Smoothing *B/A* for estimating $\langle Vp \rangle / \langle Vs \rangle$

The ratio *B/A* is calculated by using the unsmoothed data of both *A* and *B* and then the resulted data is filtered by applying the same smoothing criteria as done previously. The smoothed *B/A* data is then applied to estimate the average *Vp/Vs*.

3.7.3 Smoothing ⟨*Vp*⟩/⟨*Vs*⟩

Finally, in this scenario, the ⟨*Vp*⟩/⟨*Vs*⟩ ratios estimated at the end of the modelling are smoothed and then visualized for both the span conditions.

At the end, the smoothing criteria from which the best desired results are achieved would then be applied for the estimation of ⟨*Vp*⟩/⟨*Vs*⟩ ratios in VTI media.

4 Results

4.1 Background trends comparison

The background trends for both the isotropic and VTI media are shown in Figure 5. The solid lines represent the isotropic media whereas the dotted lines portray the VTI media. The background trend for both the cases moves anti-clockwise as *Vp* decreases or *Vp/Vs* increases. The deviation is not too much between both scenarios since a weak anisotropy is involved assuming clay content of 50%. Therefore, no significant difference is observed for background trends between isotropic and VTI media.

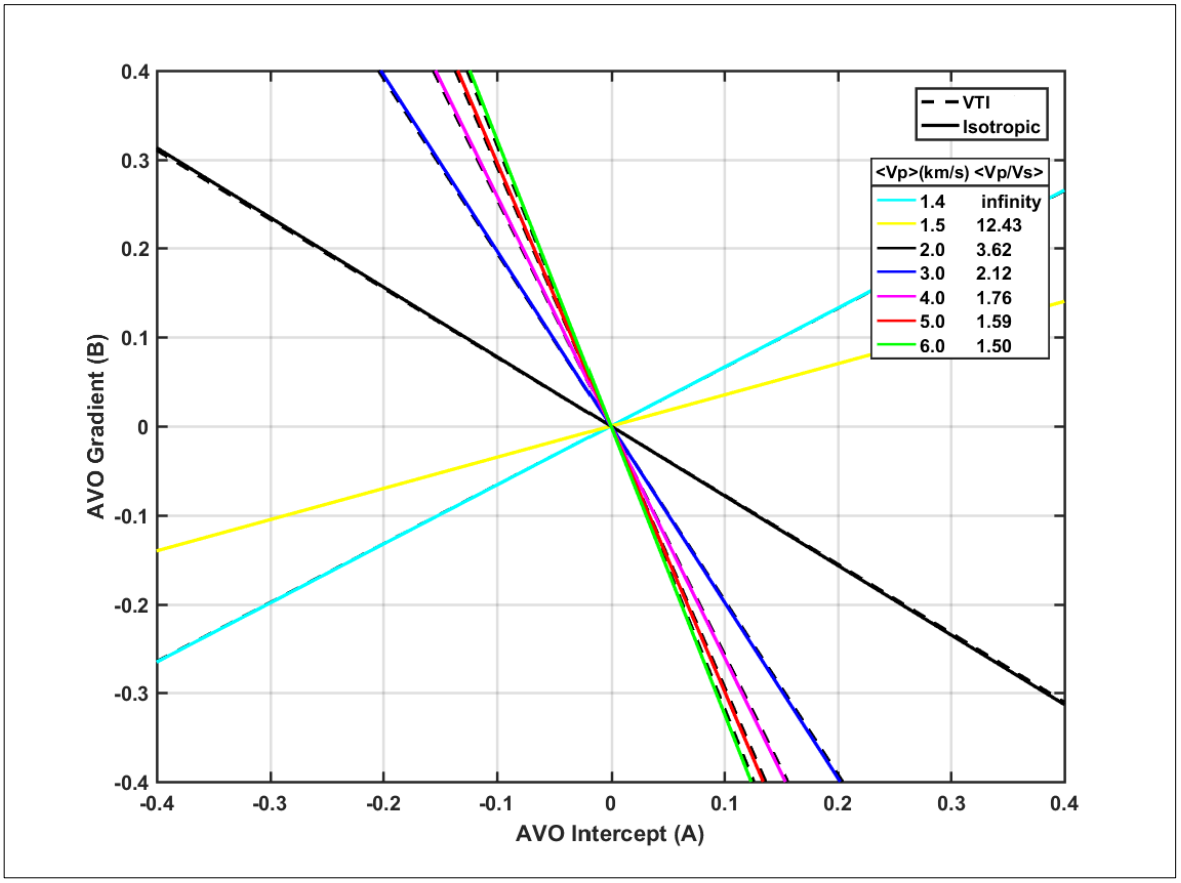

Figure 5. Intercept versus gradient comparison for isotropic and VTI media assuming a linear *Vp* versus *Vs* trend (m = 1.16, c = 1.36 km/s, g = 0.25, V_{clay} = 0.5, assumed, equation (34).

4.2 Plane-wave reflection coefficient as function of angle of incidence in isotropic and VTI media

Figure 6 shows the results produced using two term approximation, (Rüger, 1997) and Castagna et al. (1998) model parameters. Castagna et al. (1998) modelling shows significant

changes in both the circumstances reviewed in the diagram. The upper red curve represents the positive weak anisotropy whereas the lower red curve shows the negative weak anisotropy. The deviation in both the isotropic and VTI media starts approximately at an angle of incidence of 5 degrees, becoming more prominent with the increase in angle. The plot represents AVO Class IV since it has a negative intercept (*A*) and positive gradient (*B*).

Similarly, the bottom plot shows the comparison between isotropic and anisotropic material using (Rüger, 1997) model parameters. Here, an entirely opposite result is obtained with the inclusion of anisotropy, changing the negative gradient in isotropic case to positive gradient in a VTI media, showing its significance.

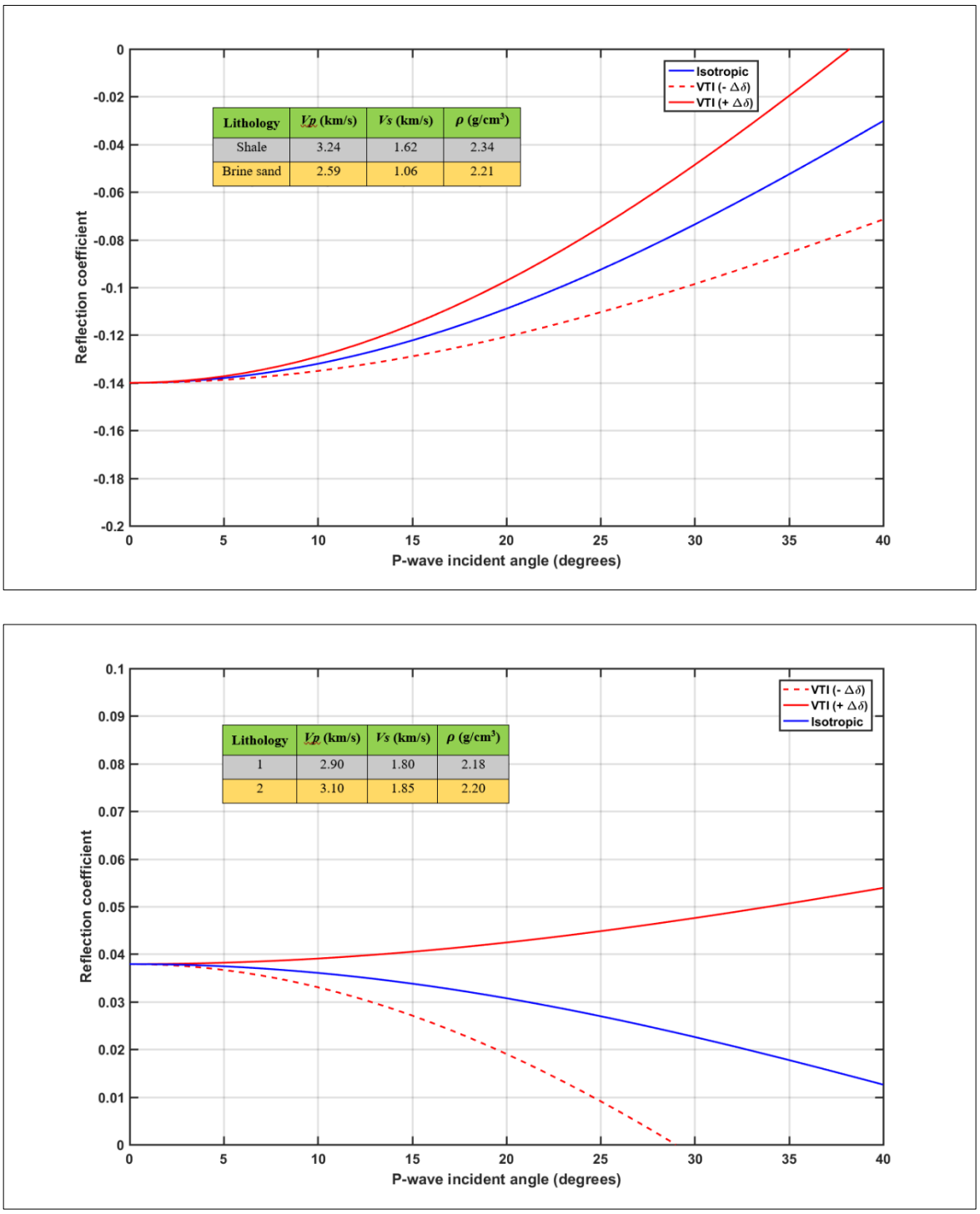

Figure 6. Plane-wave reflection coefficient versus the angle of incidence for isotropic and VTI media using the two-term approximation, assuming $\Delta\delta = \pm 0.2$. Castagna et al. (1998) (top) and Rüger (1997) (bottom).

4.3 Estimated average *Vp/Vs* from *B/A* using log based well data

As mentioned in previous chapter, different smoothing cases were involved to evaluate the average *Vp/Vs* ratios. The best desired results for ⟨*Vp*⟩/⟨*Vs*⟩ ratios in isotropic media were obtained by using the smooth function for *B/A* compared to the other scenarios, shown in Appendix D. Therefore, the same *B/A* smoothing criteria was applied to determine the ⟨*Vp*⟩/⟨*Vs*⟩ ratios in a VTI media as well.

4.3.1 Estimating ⟨*Vp*⟩/⟨*Vs*⟩ from smoothing data *B/A* in isotropic media

As explained in previous chapter, using the unsmoothed data of both *A* and *B*, the ratio *B/A* is calculated and then smoothed by applying the smoothing function. The outcome for both the wells are shown in Figure 7 and Figure 8 respectively.

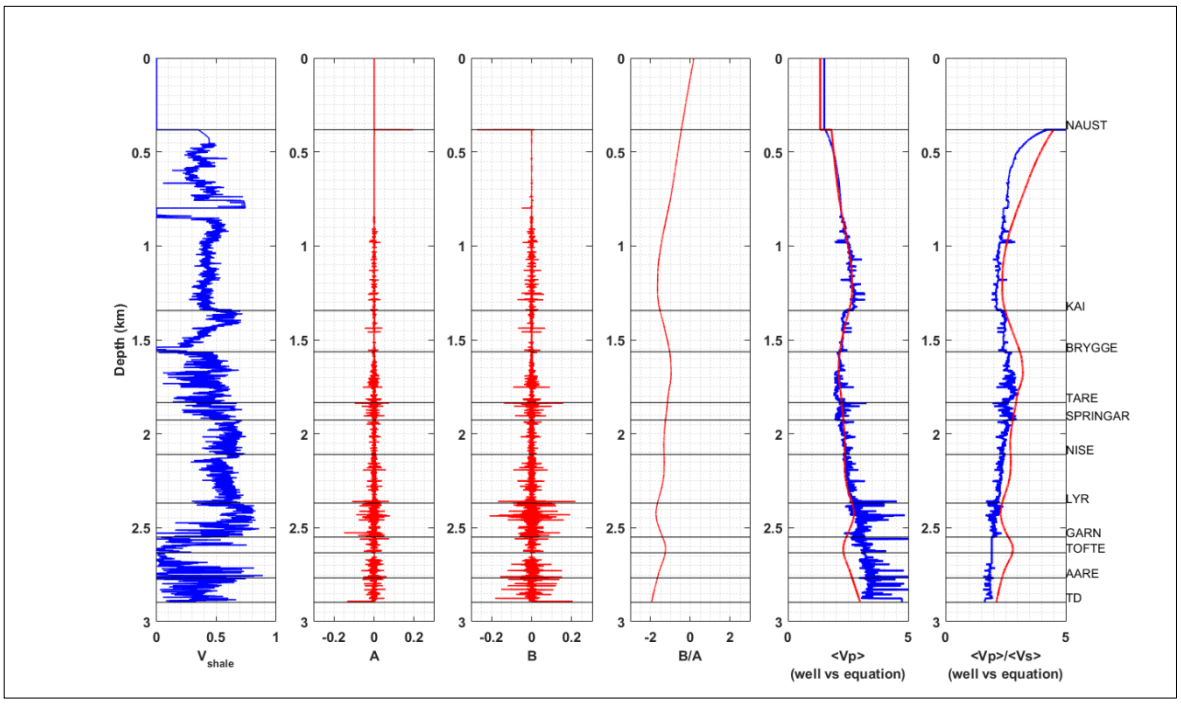

Figure 7. ⟨*Vp*⟩ and ⟨*Vp*⟩/⟨*Vs*⟩ estimated by smoothing the response data *B/A* using span of 2001 and constant *m*, *g* and *c* (assuming V_{sh} = 50%) in isotropic media. Well 6608/10-3, Norne Field.

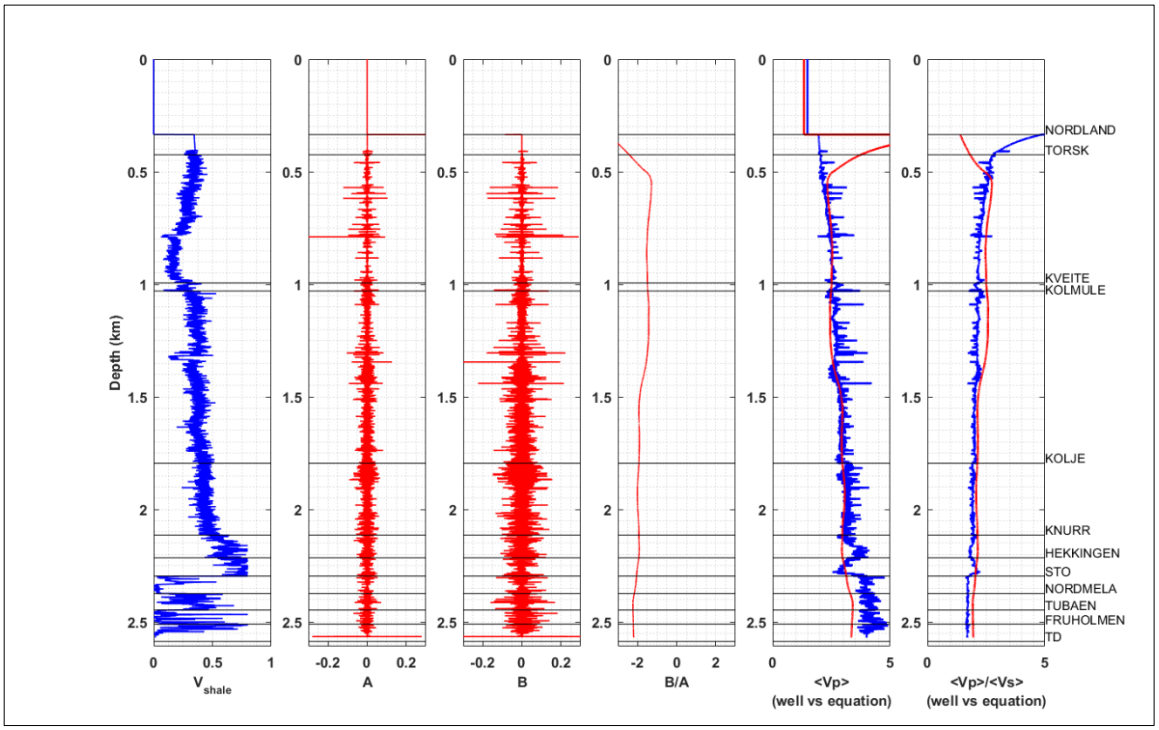

Figure 8. ⟨*Vp*⟩ and ⟨*Vp*⟩/⟨*Vs*⟩ estimated by smoothing the response data *B/A* using span of 2001 and constant *m*, *g* (assuming V_{sh} = 50%) in isotropic media. Well 7121/4-1, Snøhvit Field.

4.3.2 Estimating ⟨*Vp*⟩/⟨*Vs*⟩ from smoothing data *B/A* in VTI media

Since the best desired results for ⟨*Vp*⟩/⟨*Vs*⟩ in isotropic media were obtained by using the smooth function for *B/A* compared to the other scenarios, therefore, the same *B/A* smoothing criteria was applied to determine the ⟨*Vp*⟩/⟨*Vs*⟩ in a VTI media for both (Li, 2006) and (Ryan-Grigor, 1997) modelling parameters. The output for this case using third order polynomial, cubic equation (34) is represented in Figure 9 for well 6608/10-3, Norne Field.

As shown in plot, no significant difference is seen for both (Li, 2006) and (Ryan-Grigor, 1997) modelling scenario for estimating ⟨*Vp*⟩. Therefore, the rest of the modelling was done using (Li, 2006) modelling parameters only.

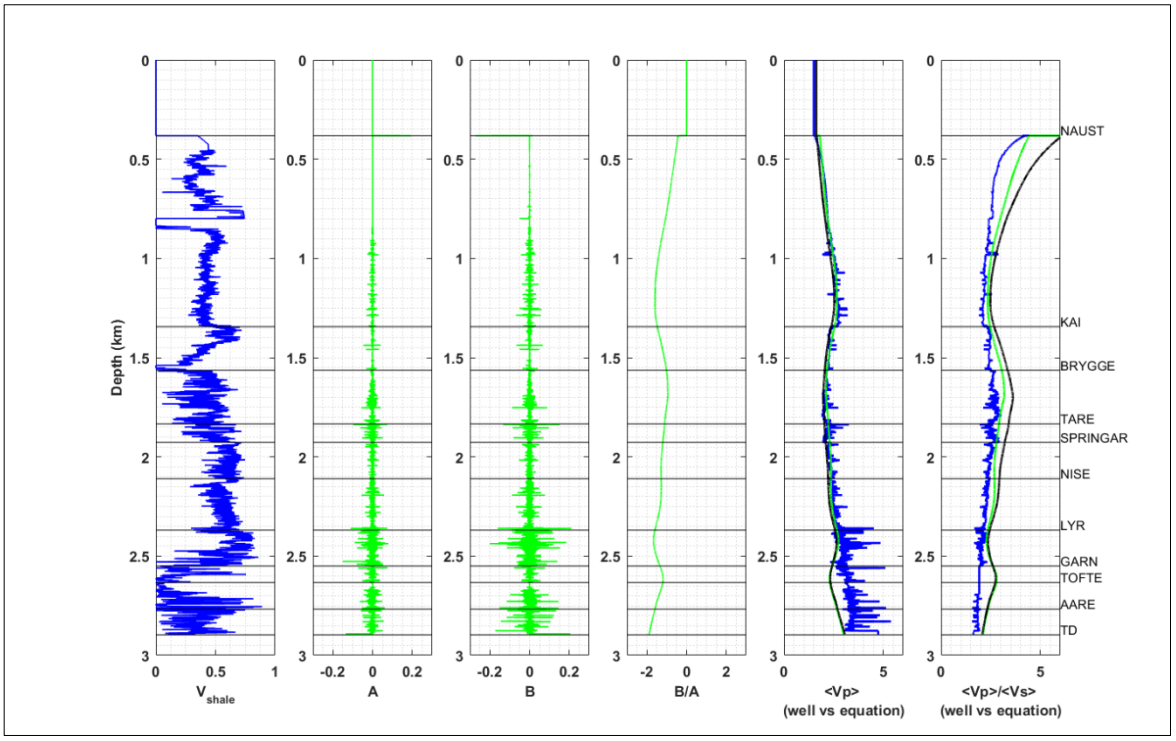

Figure 9. ⟨*Vp*⟩ and ⟨*Vp*⟩/⟨*Vs*⟩ estimated by smoothing the response data *B/A* using span of 2001 and constant *m*, *g* and *c* (assuming V_{sh} = 50%) in a VTI media using equation (34). Green = (Li, 2006) and black = (Ryan-Grigor, 1997), Well 6608/10-3, Norne Field.

Similarly, Figure 10 shows the outcome for the well 7121/4-1, Snøhvit Field.

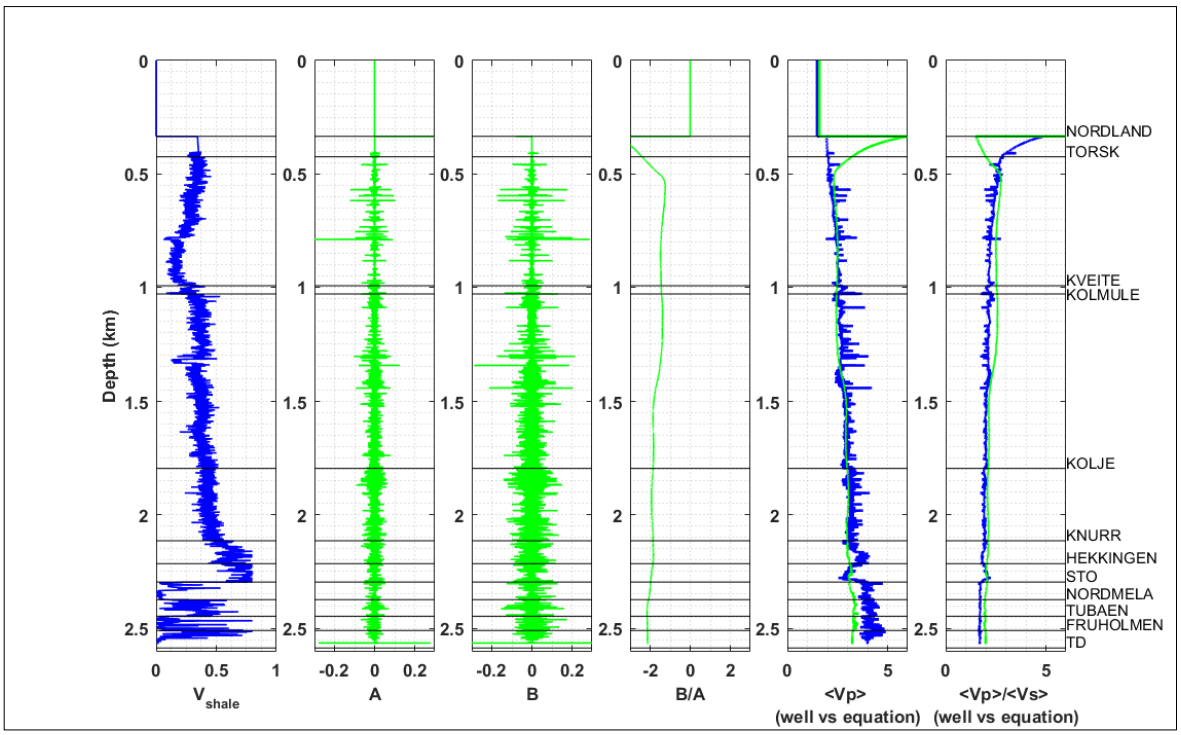

Figure 10. ⟨*Vp*⟩ and ⟨*Vp*⟩/⟨*Vs*⟩ estimated by smoothing the response data *B/A* using span of 2001 and constant *m*, *g* and *c* (assuming V_{sh} = 50%) in a VTI media, using equation (34). Well 7121/4-1, Snøhvit Field.

4.3.3 Comparison of ⟨*Vp*⟩/⟨*Vs*⟩ ratios between isotropic and anisotropic (VTI) media using log based well data

The best desired results are obtained by using the smoothing condition *B/A* using span of 2001 and constant *m*, *g* and *c* values as mentioned previously. Figure 11 shows the plots produced for both the isotropic and VTI media of wells 6608/10-3 and 7121/4-1. The blue curve shows the ⟨*Vp*⟩/⟨*Vs*⟩ ratios obtained from the synthetic well data whereas the red and green curves represent the ⟨*Vp*⟩/⟨*Vs*⟩ ratios obtained through modelling, using the equation (22) and equation (34) for isotropic and VTI media, respectively. The comparison for both the estimated and well log curves starts from depth of 800 m to 2500 m for the well 6608/10-3 whereas for well 7121/4-1, it starts from depth of 500 m to 2300 m; shown by horizontal orange solid lines. The data of intercept and gradient before this starting depth of comparison is assumed to be insufficient, very low in values. However, the overall trend of the modelled curves in both the isotropic and VTI media is quite good as it follows the same direction as the one by well log data. The separation between the isotropic and VTI modelled curves is almost negligible. The estimated ⟨*Vp*⟩ overlaps with the well log ⟨*Vp*⟩ in both wells for VTI media. Nevertheless, some

minor separation is still noticeable between the modelled ⟨*Vp*⟩/⟨*Vs*⟩ curves and the well log curves. This is due to the presence of clay content which is involved in calculating the ⟨*Vp*⟩/⟨*Vs*⟩ ratios dependent on values of *m, g* and *c*. When *B/A* approaches to zero, the ⟨*Vp*⟩/⟨*Vs*⟩ ratios then rely entirely on *m, g* and *c* values.

Furthermore, there is no significance change observed in the ⟨*Vp*⟩/⟨*Vs*⟩ curves for both the isotropic and VTI conditions comparison. The possible reason for this is due to the weak anisotropy involved as shown in the anisotropic well logs in Figure 1 and Figure 2. Since the anisotropy parameter delta 'δ' is only involved for calculating the ⟨*Vp*⟩/⟨*Vs*⟩ in a VTI media, its values are quite small, with the average around 0.03 as shown in Figure 1 and Figure 2. That's the reason there is almost no change can be seen in both the isotropic and VTI curves.

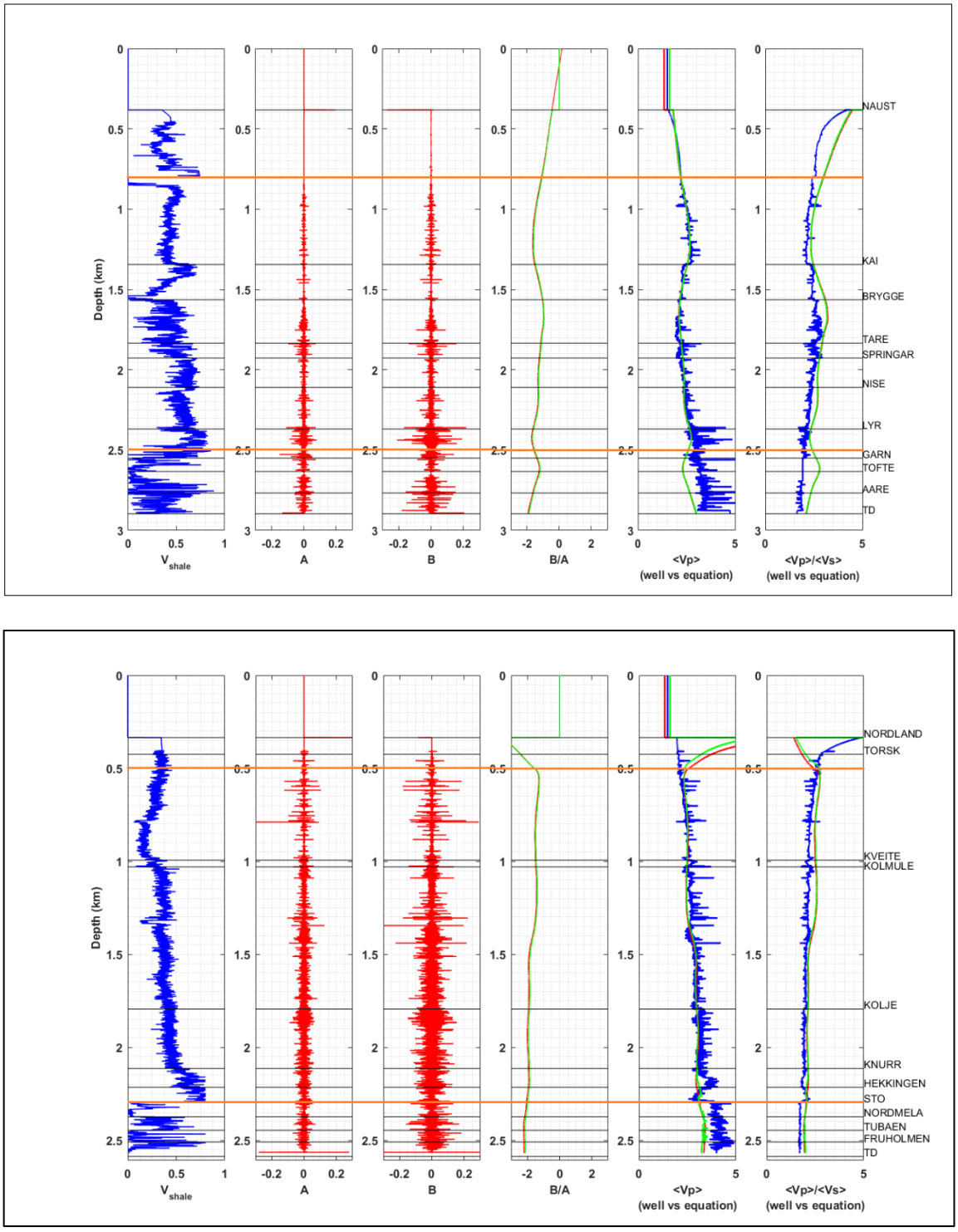

Figure 11. ⟨*Vp*⟩ and ⟨*Vp*⟩/⟨*Vs*⟩ estimated by smoothing the response data *B/A* using span of 2001 and constant *m*, *g* and *c* (assuming V_{sh} = 50%) for isotropic (red) and VTI (green) media. Well 6608/10-3, Norne Field (top) and Well 7121/4-1, Snøhvit Field (bottom).

4.4 Estimated average *Vp/Vs* from *B/A* using synthetic seismogram

Likewise, in previous section, the same procedure and conditions were followed including smoothing scenarios for the estimation of ⟨*Vp*⟩/⟨*Vs*⟩ using synthetic seismogram in GEOVIEW. However, since the data values for *A* and *B* had now been decreased to 2906 compared to 18892 samples of the well 6608/10-3 data calculated in previous section, so the span values were adjusted respectively by using simple ratio method for both wells.

4.4.1 Comparison of ⟨*Vp*⟩/⟨*Vs*⟩ ratios between isotropic and anisotropic (VTI) media using synthetic seismogram

The best appropriate results are again achieved by applying the smoothing condition *B/A* using span of 309 and constant values of *m*, *g* and *c*. However, now the values of *A* and *B* are presented in the form of wavelet since they were extracted after doing the AVO synthetics using Ricker wavelet of 25 Hz in GEOVIEW. Again, we can see a good result for the modelled ⟨*Vp*⟩/⟨*Vs*⟩ data for both the isotropic and VTI conditions against the well log ⟨*Vp*⟩/⟨*Vs*⟩ ratios, shown in Figure 12. For the comparison between them, the same approach is used as done previously. Similarly, like before, the general trend for both the scenarios is same, i.e., no significant change is seen in both isotropic and VTI media. However, more contrast, separation is observed between the well log ⟨*Vp*⟩/⟨*Vs*⟩ curve and modelled ⟨*Vp*⟩/⟨*Vs*⟩ curve. The main reason for this separation is due to the smoothing of the data and frequency bandwidth problem, shown in Appendix F. By using the Ricker wavelet of 25 Hz and smoothing function, more data values are eaten out, neglected. Therefore, the smoothing condition and seismic frequency bandwidth problem both effects the curve trend when doing the stability of the model. Anisotropic parameters, delta and epsilon are present as well but since their values are very small they are not creating significant changes compared to isotropic situation as the anisotropy is quite small, weak.

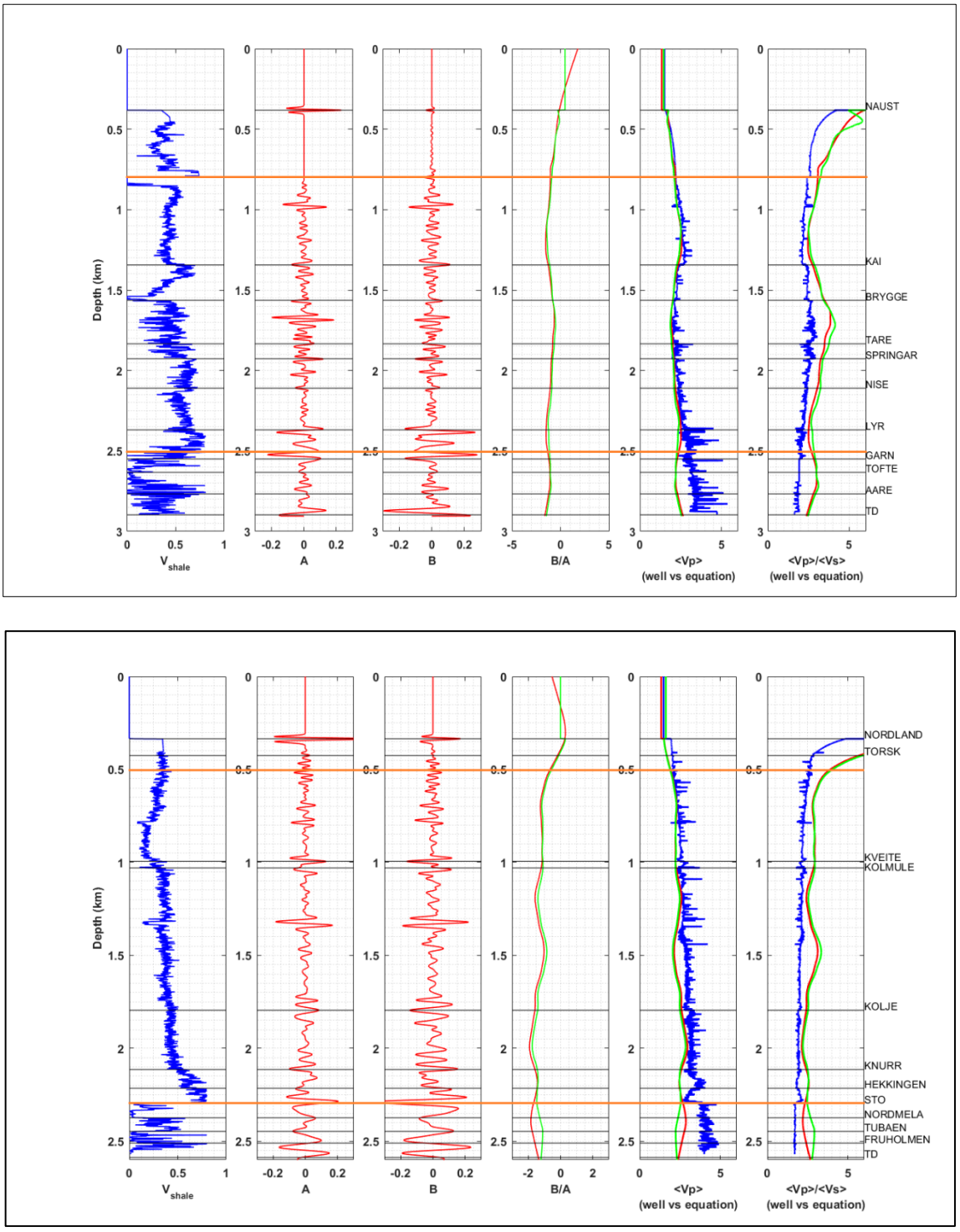

Figure 12. ⟨*Vp*⟩ and ⟨*Vp*⟩/⟨*Vs*⟩ estimated by smoothing the response data *B/A* using span of 309 and constant *m*, *g* and *c* (assuming V_{sh} = 50%) for isotropic (red) and VTI (green) media. Well 6608/10-3, Norne Field (top) and Well 7121/4-1, Snøhvit Field (bottom).

4.5 Estimated average *Vp*/*Vs* from *B/A* using real seismic data

The real seismic 2D data of Norne Field was used for estimation of average *Vp* and *Vp/Vs* ratios across the whole data section (CMP = 1300 - 2300). Figure 13 shows the outcome at well location, i.e., inline = 1045, xline = 1829 and at another position of inline = 1045, xline = 2100. The results for more different locations are given in Appendix E.

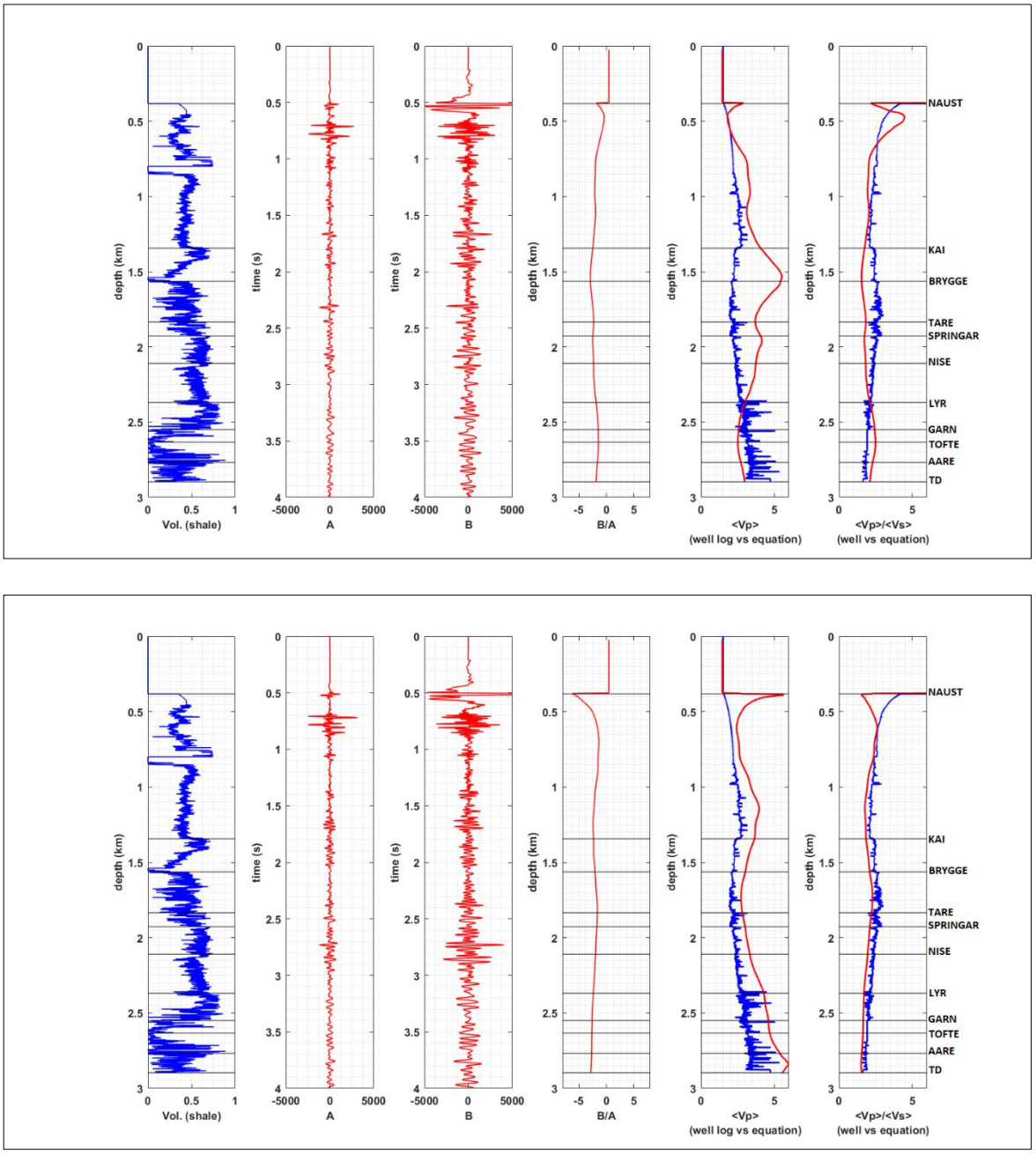

Figure 13. ⟨*Vp*⟩ and ⟨*Vp*⟩/⟨*Vs*⟩ estimated by smoothing the seismic response data *B/A* and constant *m*, *g* and *c* (assuming V_{sh} = 50%) for VTI media using equation (34), Norne Field. Inline = 1045, xline = 1829 (top) and inline = 1045, xline = 2100 (bottom).

Like previously, the same depth window would be used for comparison as before, i.e., from 800 m to 2500 m. The best outcome of all the locations for the estimated average *Vp* and *Vp/Vs* ratios across the whole data section is obtained at inline = 1045 and xline = 2100. At this position, the trend of both the estimated curves follow the same trend as that of well data curves. However, significant deviations, fluctuations between the estimated curves and the well data curves can be easily seen at different locations. The possible reason for this is the seismic data resolution, frequency, and bandwidth. The frequency of well data is infinite compared to seismic data of 25 Hz dominant frequency using Ricker wavelet. Furthermore, higher frequency data gets muted when using Ricker wavelet as well, resulting in less data values and more fluctuation of estimated curves. This frequency dependence problem is investigated and the results at different dominant frequencies are given in Appendix F. Moreover, the average *Vs* well data values are synthetic, predicted ones which would affect the average *Vp/Vs* ratios as well.

Figure 14, Figure 15 and Figure 16 show the cross sections of the intercept, gradient and their ratios '*B/A'*, estimated average *Vp* and *Vp/Vs* ratios across the whole 2D line of seismic data.

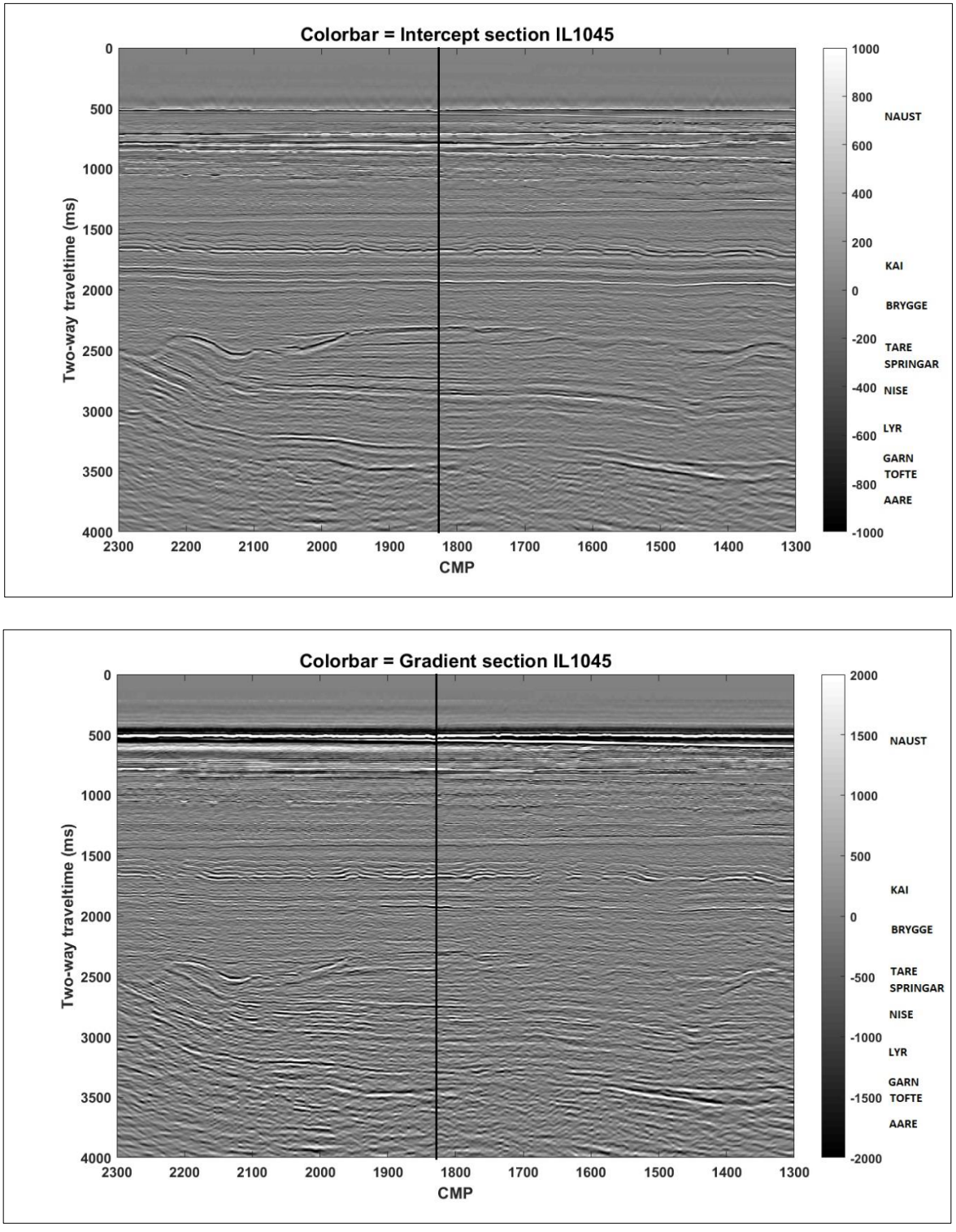

Figure 14. Intercept and gradient cross section for estimation of ⟨*Vp*⟩ and ⟨*Vp*⟩/⟨*Vs*⟩ ratios across the whole 2D seismic line. Black vertical line represents well location.

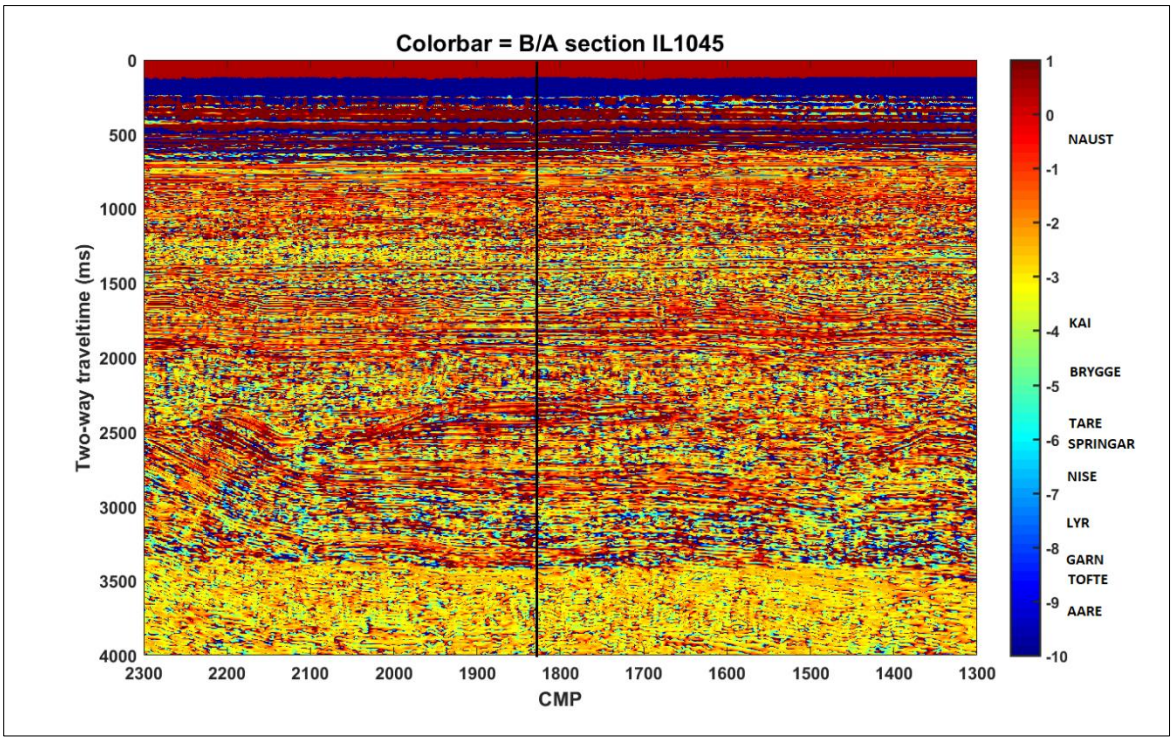

Figure 15. Estimated *B/A* cross section for modelling of ⟨*Vp*⟩ and ⟨*Vp*⟩/⟨*Vs*⟩ ratios across the whole 2D seismic line. Black vertical line represents well location.

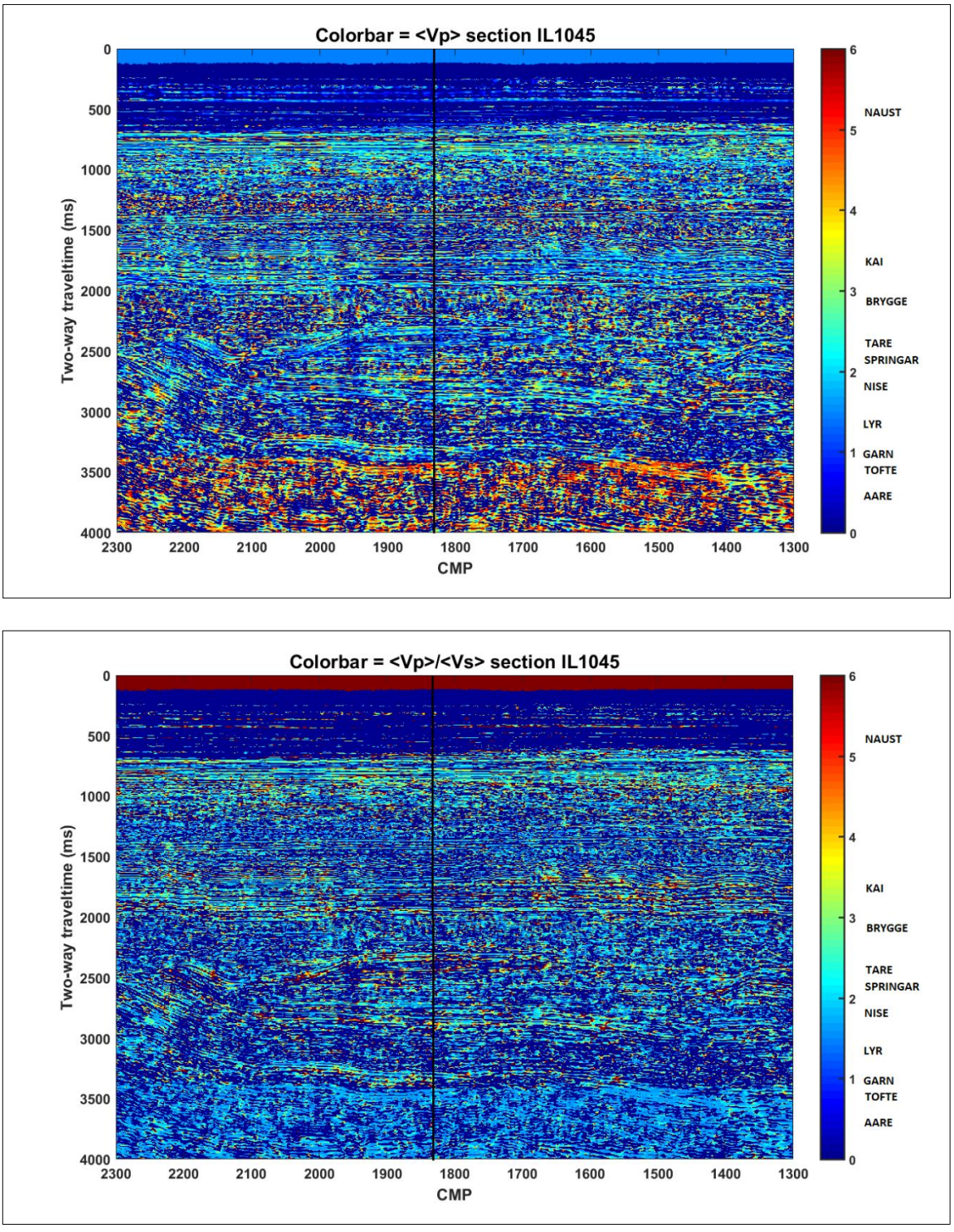

Figure 16. Estimated $\langle Vp \rangle$ and $\langle Vp \rangle / \langle Vs \rangle$ cross sections of the seismic response data *B/A* and constant *m*, *g* and *c* (assuming V_{sh} = 50%) for VTI media using equation (34), Norne Field. Black vertical line represents well location.

In the sections produced, data before two-way traveltime of 550 ms approximately, is insufficient due to the muting process when generating the stack sections of gradient and intercept. The estimated sections are produced using the same smoothing conditions as before in MATLAB. However, the sections appeared noisy but still correct as the data values are in the same range as that of the well log data. The reason for this noisiness is again due to the seismic frequency, bandwidth problem which creates fluctuations in the modelled average *Vp* and *Vp/Vs* data values as explained before, shown in Appendix E and Appendix F. Also, the *Vp* and *Vp/Vs* sections produced are resulted from 1000 individual *B/A* sections across the whole 2D line.

5 Discussion

An AVA background trend defined as function of intercept and gradient crossplot plays a significant role for detecting hydrocarbon reservoirs. With the increase in $\langle Vp \rangle / \langle Vs \rangle$ ratio, the background trend *B/A* starts rotating counter clockwise in both the isotropic and anisotropic media (VTI symmetry). However, the separation between the background trends in isotropic and VTI media is negligible, assuming weak VTI anisotropy. This is due to the parameter '$\Delta\delta$' using equation (29) which is the contrast in delta values of upper layer and lower layer across the interface of different lithologies, not between individual layers of same lithology. However, if we assume $\Delta\delta = 0.2$ then significant difference would be observed. Furthermore, we have seen more prominent anisotropic effect in Figure 6 when doing reflectivity modelling using equation (5) where a material with negative gradient in isotropic case converts to a positive gradient in a VTI condition, exhibiting importance of anisotropy.

The intercept term '*A*' for both the isotropic and VTI conditions remains the same since it is not affected by anisotropy. Therefore, the anisotropic effects in VTI media are caused by the gradient term '*B*' only which includes the anisotropic parameter delta 'δ'. Moreover, the values of parameters 'δ' and 'ε' used are predicted ones, not measured values.

In general, the trend of the modelled $\langle Vp \rangle$ and $\langle Vp \rangle / \langle Vs \rangle$ curves in both the isotropic and VTI media using log based data appears to be remarkably good. The modelled $\langle Vp \rangle$ curve in both media overlaps with the well $\langle Vp \rangle$ data for both Norne and Snøhvit Fields.

The anisotropic synthetic seismic CMP gathers produced showed negligible changes in reflection amplitude when compared to isotropic case for both wells. The possible reason for this is due to the weak anisotropy involved. The delta of the well data calculated by implementing equation (23) turns out to be very low, with average value around 0.02 in magnitude as can be seen in Figure 1 and Figure 2; resulting in no outstanding differences in the synthetic seismic CMP gathers generated.

The results obtained from synthetic seismogram were also relatively reasonable but not as precise like log based only. As explained in previous chapter, the feasible reason for this change is the frequency dependence problem. The frequency of synthetic well data is infinite compared to normal seismic data of 25 Hz frequency. The data values of *A* and *B* are generated with the assumption of 25 Hz dominant frequency, Ricker wavelet. Therefore, the modeled curves using synthetic seismograms are more fluctuating ones compared to modelled curves using log based data. Moreover, the *Vs* data of both wells is predicted, synthetic one which affect the average *Vp* and *Vp/Vs* ratios as well.

Another plausible explanation for this fluctuation in modelled ⟨*Vp*⟩ and ⟨*Vp*⟩/⟨*Vs*⟩ curves is the consequence of smoothing of the well data which changes the shape of the curve at different low and high span values. Smoothing tends to remove the inappropriate data, for example, *B/A* = 0 or infinity, which appeared to be present in *B/A*, creating instability problem as well. Therefore, one should investigate this smoothing filter function to obtain the optimal span values so that the results achieved are more realistic with respect to the original data. Of all the smoothing scenarios used in this study, the best smoothing case is the one in which ⟨*Vp*⟩ and ⟨*Vp*⟩/⟨*Vs*⟩ data estimated by smoothing data of *B/A* only.

Nevertheless, the estimated ⟨*Vp*⟩ and ⟨*Vp*⟩/⟨*Vs*⟩ curves in isotropic and VTI media overlaps with each other. Only negligible separation can be seen between both the cases. Again, the possible reason for this negligible separation of curves is due to the involvement of small weak contrast approximation, using anisotropic parameter δ only. Furthermore, the relationship between delta and epsilon, equation (23), is resulted from the best fit line of δ against ε, Li (2006).

The estimated results obtained for average *Vp* and *Vp/Vs* curves using seismic intercept and gradient sections were quite good as well at different locations along the 2D seismic line. The fluctuations between the modelled and well curves resulted due to seismic frequency, bandwidth problem and smoothing function as well. The average *Vp* and *Vp/Vs* sections produced at the end appeared to be noisy but still reasonably good, satisfactory as well as the data values are in the same range as that of the well data. Also, another important thing to be aware of is that the seismic data used is the result of seismic reflectivity convolved with a seismic wavelet. These are, therefore, seismic amplitudes and they are not equal to seismic reflectivity.

6 Conclusions

Estimation of average *Vp* and *Vp/Vs* ratios in isotropic and VTI media using AVA attributes is a task with numerous difficulties and challenges. In this thesis, explicit equations have been derived for the estimation of average *Vp* and *Vp/Vs* ratios in isotropic and VTI media, respectively.

Anisotropic effects assuming VTI symmetry are being compared in relation to isotropic properties on *B/A* background trends and reflectivity. The *B/A* background trends in both the cases rotates counter clockwise with increase in $\langle Vp \rangle / \langle Vs \rangle$ ratios. But, negligible separation is observed between both the isotropic and VTI media. However, P-wave reflection coefficient modelling in isotropic and VTI media shows significant differences, demonstrating the importance of anisotropy.

The expressions derived for the estimation of average *Vp* and *Vp/Vs* ratios from *B/A* using log based data gives remarkable results when compared to the well log data. However, exact and precise results were not obtained though when doing the modelling using synthetic seismograms *B/A* data values and real seismic *B/A* sections of a 2D seismic line. This is due to seismic frequency bandwidth problem, smoothing function effects and instability problem as well. Furthermore, one should keep in mind that the average *Vs* well data values used are synthetic, predicted ones which affect the average *Vp/Vs* ratios as well.

The estimated $\langle Vp \rangle / \langle Vs \rangle$ deviation for isotropic and anisotropic (VTI) media was not quite prominent due to very small, weak anisotropy involved; low data values of delta and epsilon which are predicted ones, not measured values.

Smoothing filter function plays an essential role for stabilizing the average *Vp* and *Vp/Vs* ratios modelling. But its optimal parameters should be investigated to get the reliable and realistic results since a lot of original data get neglected during the process of achieving the perfect fit between the modelled $\langle Vp \rangle / \langle Vs \rangle$ curve and well logged $\langle Vp \rangle / \langle Vs \rangle$ curve. Likewise, seismic frequency bandwidth problem is important as well regarding stability and precision of the estimated data.

Estimation of average *Vp* and *Vp/Vs* ratios from AVA attributes is possible and gives remarkable results if all the challenges are understood, handled properly for this task.

7 Future work

This study was based using the weak contrast two term approximation only. Therefore, one should carry out the same procedure using the third term which involves the parameter gamma *'γ'* to see how the results differentiate when being compared to two term weak contrast approximation. Also, the smoothing function and frequency bandwidth problems should be investigated furthermore to find their optimal parameters.

8 References

AKI, K. & RICHARDS, P. G. 1980. *Quantitative Seismology: Theory and Methods*, W. H. Freeman.

ALKHALIFAH, T. & RAMPTON, D. 2001. Seismic anisotropy in Trinidad: A new tool for lithology prediction. *The Leading Edge,* 20**,** 420-424.

BANIK, N. C. 1987. An effective anisotropy parameter in transversely isotropic media. *GEOPHYSICS,* 52**,** 1654-1664.

CASTAGNA, J. P., BATZLE, M. L. & EASTWOOD, R. L. 1985. Relationships between compressional-wave and shear-wave velocities in clastic silicate rocks. *GEOPHYSICS,* 50**,** 571-581.

CASTAGNA, J. P., SWAN, H. W. & FOSTER, D. J. 1998. Framework for AVO gradient and intercept interpretation. *Geophysics,* 63**,** 948-956.

COBDEN, L., THOMAS, C. & TRAMPERT, J. 2015. Seismic Detection of Post-perovskite Inside the Earth. *In:* KHAN, A. & DESCHAMPS, F. (eds.) *The Earth's Heterogeneous Mantle: A Geophysical, Geodynamical, and Geochemical Perspective.* Springer.

GARDNER, G. H. F., GARDNER, L. W. & GREGORY, A. R. 1974. FORMATION VELOCITY AND DENSITY—THE DIAGNOSTIC BASICS FOR STRATIGRAPHIC TRAPS. *GEOPHYSICS,* 39**,** 770-780.

JOHNSTON, J. E. & CHRISTENSEN, N. I. 1995. Seismic anisotropy of shales. *Journal of Geophysical Research: Solid Earth,* 100**,** 5991-6003.

KIM, K. Y., WROLSTAD, K. H. & AMINZADEH, F. 1993. Effects of transverse isotropy on P-wave AVO for gas sands. *GEOPHYSICS,* 58**,** 883-888.

LEANEY, W. S. 1993. AVO and anisotropy from logs and walkaways. *Exploration Geophysics,* 24**,** 623-630.

LI, Y. 2006. An empirical method for estimation of anisotropic parameters in clastic rocks. *The Leading Edge,* 25**,** 706-711.

LI, Y. & PICKFORD, S. Anisotropic well logs and their applications in seismic analysis. 2002 SEG Annual Meeting, 2002. Society of Exploration Geophysicists.

MAVKO, G., MUKERJI, T. & DVORKIN, J. 2009. Empirical relations. *The rock physics handbook: Tools for seismic analysis of porous media*

Cambridge university press.

OSTRANDER, W. 1984. Plane-wave reflection coefficients for gas sands at nonnormal angles of incidence. *Geophysics,* 49**,** 1637-1648.

ROSS, C. P. 2000. Effective AVO crossplot modeling: A tutorial. *Geophysics,* 65**,** 700-711.

RÜGER, A. 1997. P-wave reflection coefficients for transversely isotropic models with vertical and horizontal axis of symmetry. *Geophysics,* 62**,** 713-722.

SHUEY, R. 1985. A simplification of the Zoeppritz equations. *Geophysics,* 50**,** 609-614.

THOMSEN, L. 1986. Weak elastic anisotropy. *Geophysics,* 51**,** 1954-1966.

WANG, Z. 2001. Seismic anisotropy in sedimentary rocks. *2001 SEG extended abstracts*.

WRIGHT, J. 1987. The effects of transverse isotropy on reflection amplitude versus offset. *Geophysics,* 52**,** 564-567.

9 Bibliography

CASTAGNA, J. P., SPRATT, R. S., GOINS, N. R., FITCH, T. J., DEY-SARKAR, S. K., SVATEK, S. V., SWAN, H. W., KAN, T. K., YOUNG, C. Y. & THOMSEN, L. 1993. 1. Principles. Offset-Dependent Reflectivity—Theory and Practice of AVO Analysis. Society of Exploration Geophysicists, pp. 1-111.

MALLICK, S., GILLESPIE, D. & SEN, M. K. 2005. Azimuthal reflectivity and quantitative evaluation of anisotropic parameters from seismic data: a feasibility study. 2005 SEG Annual Meeting.

RÜGER, A. 1998. Variation of P-wave reflectivity with offset and azimuth in anisotropic media. Geophysics, 63, 935-947.

SIMM, R., BACON, M. & BACON, M. 2014. Fundamentals. Seismic Amplitude: An interpreter's handbook. Cambridge University Press, pp. 3-22.

SIMM, R., BACON, M. & BACON, M. 2014. Rock properties and AVO. Seismic Amplitude: An interpreter's handbook. Cambridge University Press, pp. 58-149.

XU, S., KHARE, V., KEYS, B. & FINN, C. A Second Look at the Background Trend for AVO Interpretation. 2002 SEG Annual Meeting, 2002. Society of Exploration Geophysicists

APPENDIX A: Empirical coefficients

The typical values of empirical coefficients of different lithologies using density-velocity relationship, i.e., equation (7) and for a linear *Vp* versus *Vs* relationship, i.e., equation (9) are given below in Table A-1.

Table A-1. Typical values of coefficients of different lithologies for equations (7) and (9).

Lithology	***c***	***d***	***g***	***m***
Shale Mudrock (Castagna et al., 1985)	1.360	1.750	0.265	1.160
Shale (Castagna et al., 1993)	1.127	1.750	0.265	1.300
Sandstone (Castagna et al., 1993)	1.0643	1.660	0.261	1.244
Sandstone, clay > 25% (Han, 1986)	1.305	1.660	0.261	1.188
Sandstone, clay < 25% (Han, 1986)	1.326	1.660	0.261	0.871
Limestone (Castagna et al., 1993 assuming *Vp/Vs* =1.9)	8.922	1.360	0.386	-9.876
Dolomite (Castagna et al., 1993)	0.133	1.740	0.252	1.715

APPENDIX B: Well logs using GEOVIEW

The well logs (both conventional and anisotropic) produced using GEOVIEW including synthetic CMP seismic gather are shown in Figure B-1 and Figure B-2. In these plots, the clay content is represented as volume fraction.

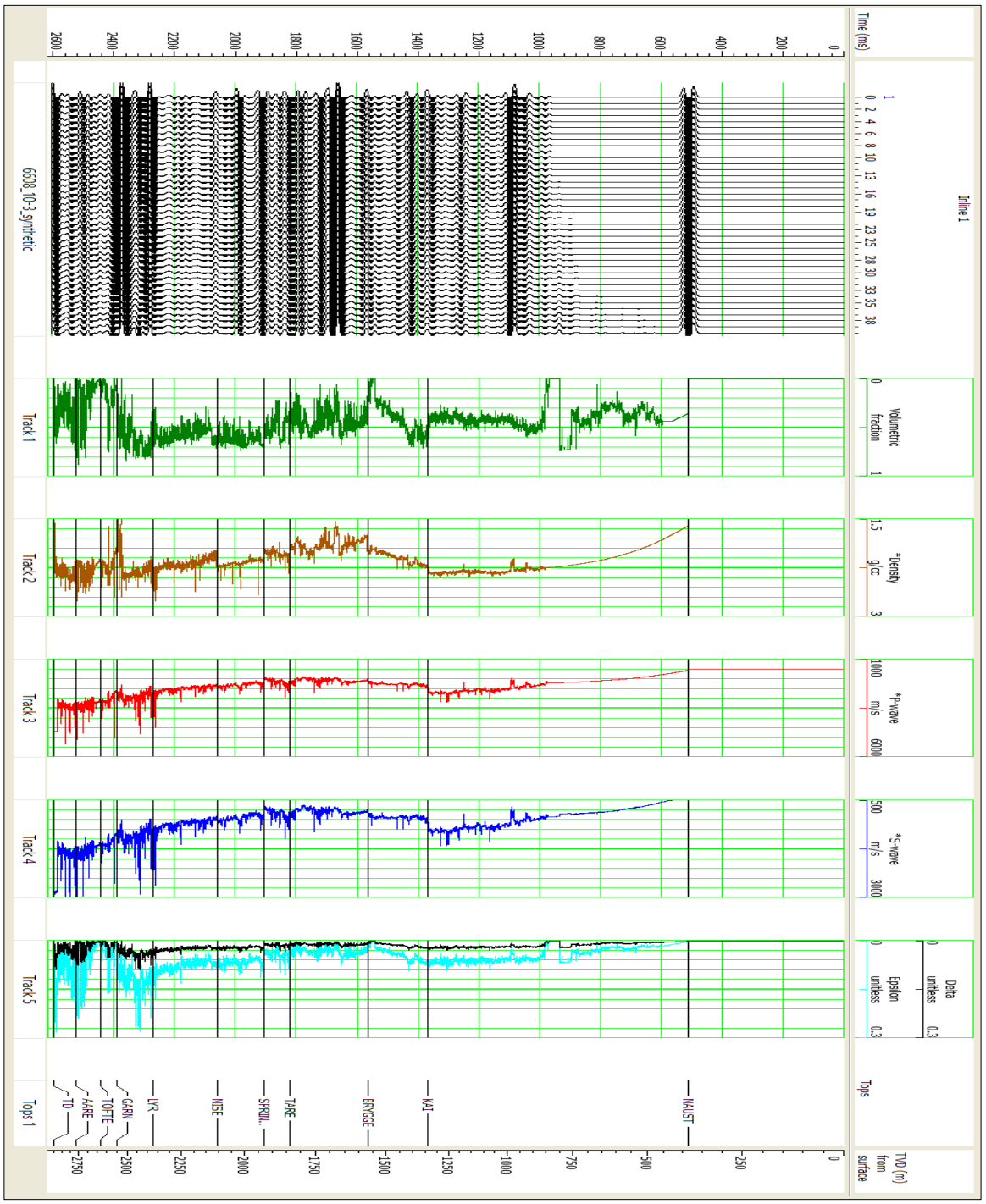

Figure B-1. Conventional well logs and estimated anisotropic well logs produced using well 6608/10-3, Norne Field on GEOVIEW.

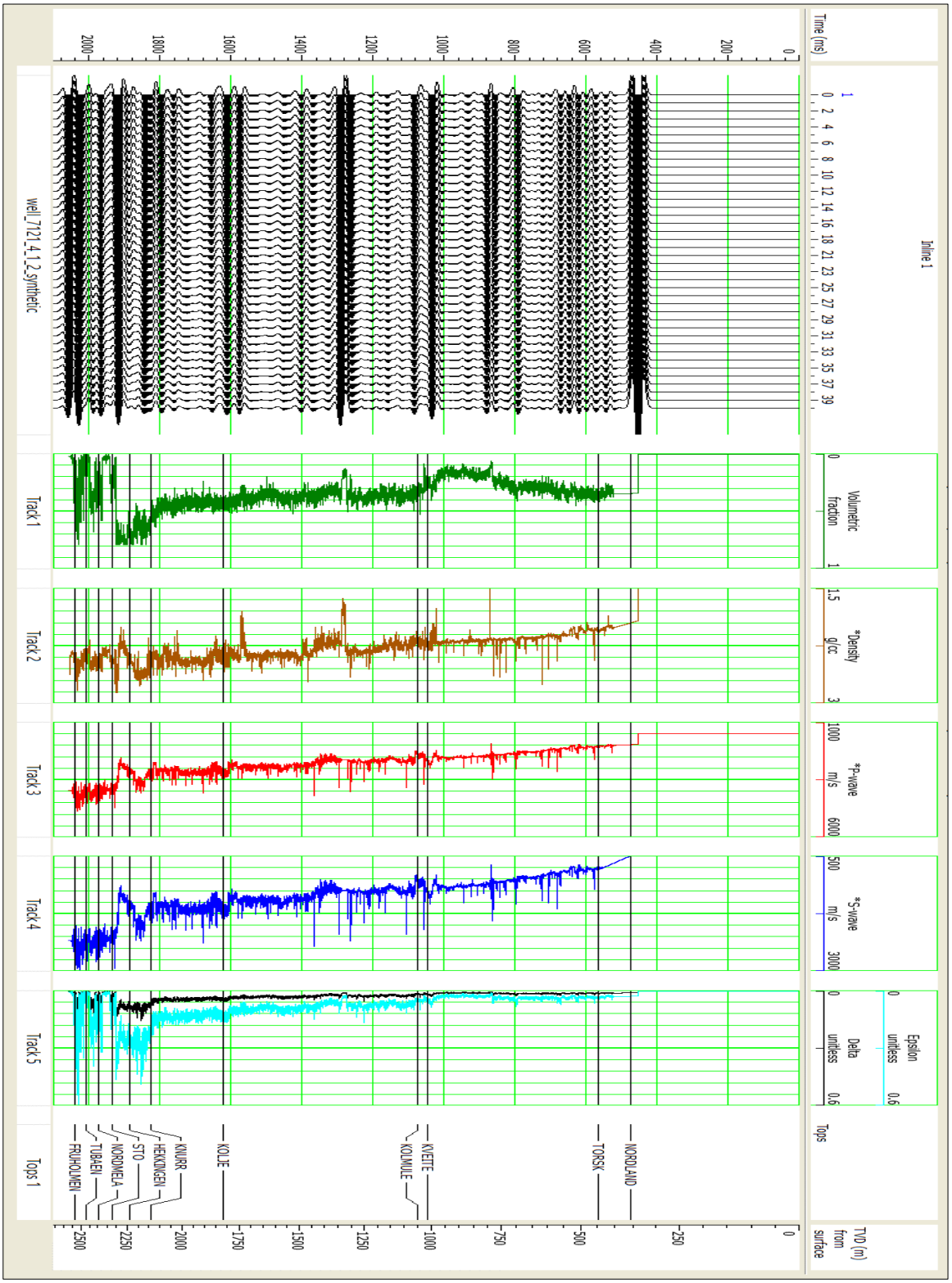

Figure B-2. Conventional well logs and estimated anisotropic well logs produced using well 7121/4-1, Snøhvit Field on GEOVIEW.

APPENDIX C: Instability problem

Equation (22) shows that the ⟨*Vs*⟩/⟨*Vp*⟩ is not only a function of *B/A* but also dependent on *m* and *g* too. If we put *B/A* = 0, then the expression becomes

$$\frac{\langle Vs\rangle}{\langle Vp\rangle} = \frac{-\frac{8}{m} + \sqrt{\left(\frac{8}{m}\right)^2 - (16g)\,(-1)}}{8g}.$$

Now, if we assume $m = 1.16 \approx 1$ and $g = 1/4$, then the expression is

$$\frac{\langle Vs\rangle}{\langle Vp\rangle} = \frac{-8 + \sqrt{68}}{2},$$

$$\frac{\langle Vs\rangle}{\langle Vp\rangle} \approx \frac{-8 + \sqrt{64}}{2},$$

and by taking inverse of it, we would get

$$\frac{\langle Vp\rangle}{\langle Vs\rangle} \approx \left(\frac{-8 + \sqrt{64}}{2}\right)^{-1},$$

$$\frac{\langle Vp\rangle}{\langle Vs\rangle} \approx \left(\frac{0}{2}\right)^{-1}$$

resulting in infinity values of ⟨*Vp*⟩/⟨*Vs*⟩ ratios. Therefore, to tackle this instability problem, smoothing function was applied to remove those data values due to which ⟨*Vp*⟩/⟨*Vs*⟩ ratios approach infinity in magnitude.

APPENDIX D: More smoothing results using log based well data

Figure D-1 shows the result acquired without applying any smoothing criteria to the log based well data. As expected, the model is quite unstable since the ratio *B/A* is both negative and positive and the calculated $\langle Vp\rangle/\langle Vs\rangle$ data is quite high as well, not allowing any comparison to be made between these two $\langle Vp\rangle/\langle Vs\rangle$ data, one from the well recorded and the other from evaluating equation (22). Consequently, it signifies the requirement for smoothing of the data and their results for different smoothing scenarios are the following.

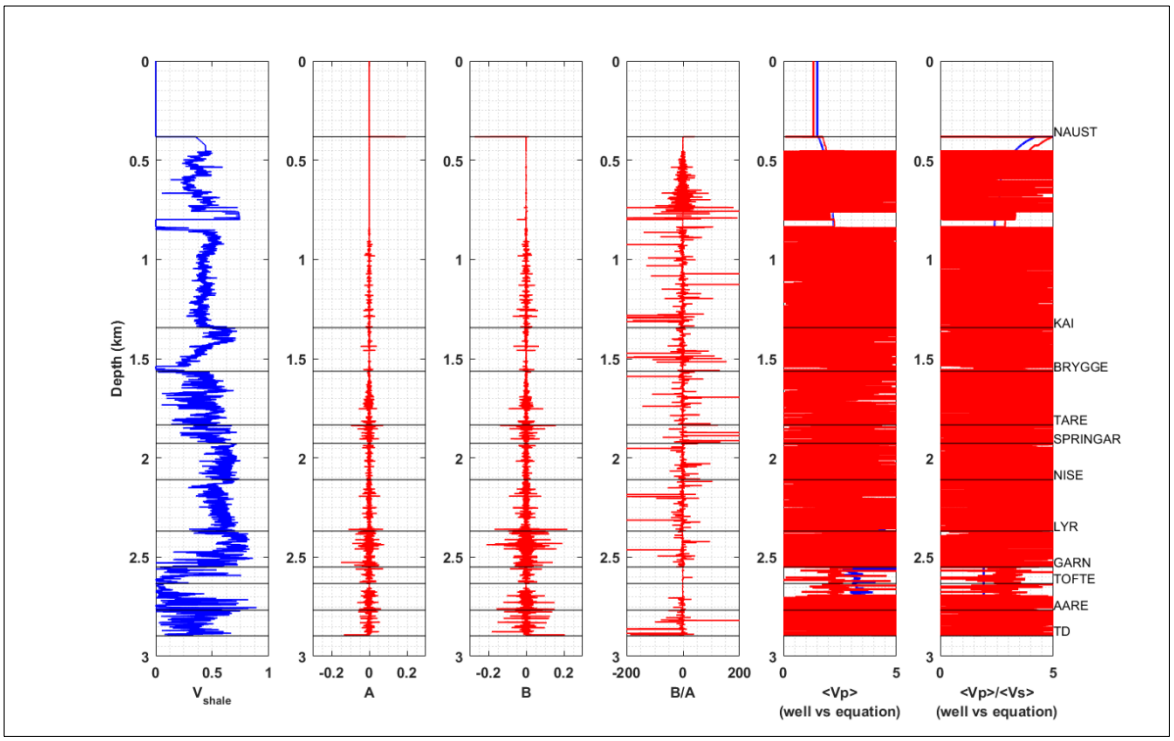

Figure D-1. Estimation of $\langle Vp\rangle$ and $\langle Vp\rangle/\langle Vs\rangle$ from *B/A* using unsmoothed data.

D.1 Estimating $\langle Vp\rangle/\langle Vs\rangle$ from smoothing data *A* and *B* in isotropic media

The smoothed data of *A* and *B* were used to calculate the ratio *B/A* which were then implemented in the equations (22) and (34) for the estimation of $\langle Vp\rangle/\langle Vs\rangle$. The results obtained from this smoothing criterion are shown in Figure D-2.

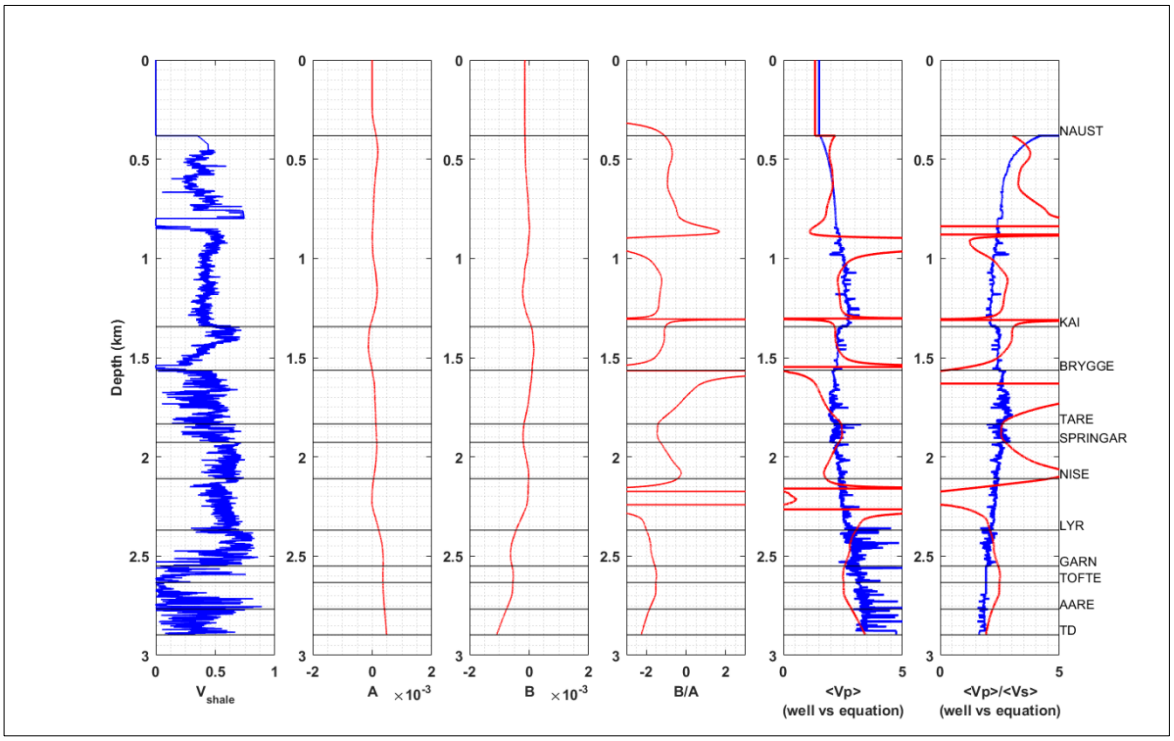

Figure D-2. ⟨*Vp*⟩ and ⟨*Vp*⟩/⟨*Vs*⟩ estimated by smoothing the response data *A* and *B* only using span of 2001 and constant *m*, *g* and *c* (assuming V_{sh} = 50%) in isotropic media. Well 6608/10-3, Norne Field.

D.2 Smoothing the estimated ⟨*Vp*⟩/⟨*Vs*⟩ data in isotropic media

The ⟨*Vp*⟩/⟨*Vs*⟩ data calculated at the end of the model was only smoothed and then plotted as shown in Figure D-3.

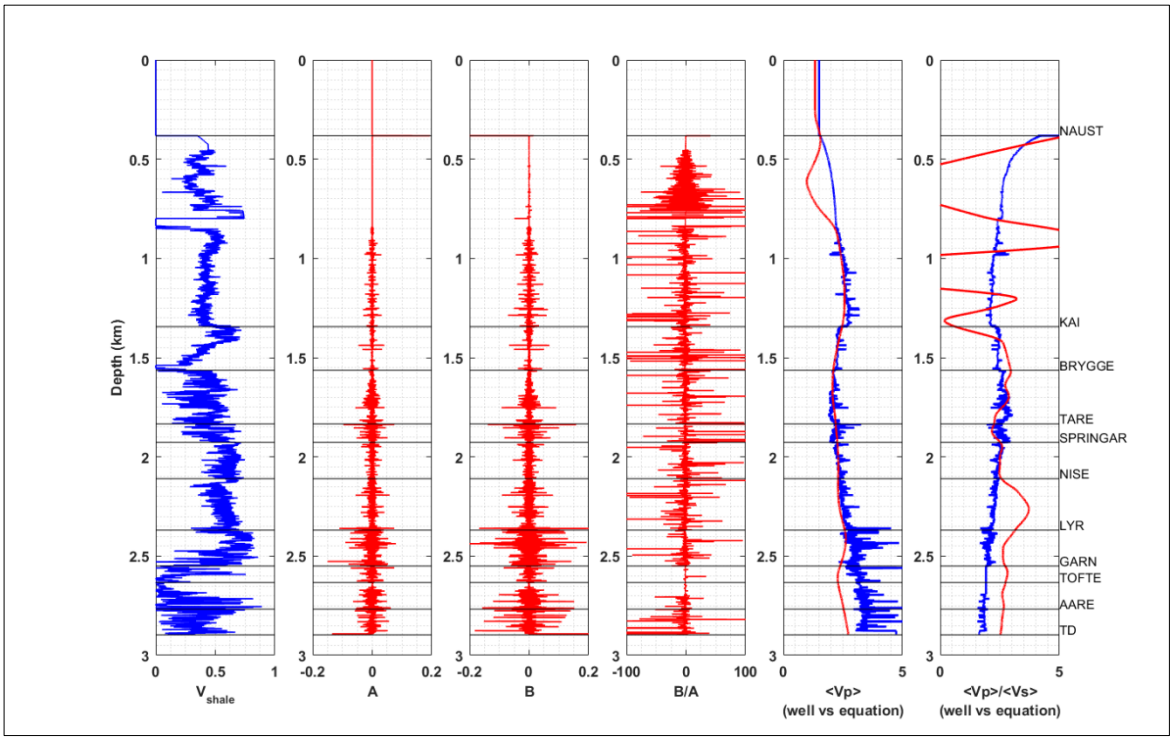

Figure D-3. Smoothed ⟨*Vp*⟩ and ⟨*Vp*⟩/⟨*Vs*⟩ calculated by using span of 2001 and constant *m*, *g* and *c* (assuming V_{sh} = 50%) in isotropic media. Well 6608/10-3, Norne Field.

More appropriate results were produced by using span of 2001 relative to lower span values in all the smoothing scenarios. However, by using higher span values, more data sample values are being taken out by the function compared to lower span values regarding the stability of the model. With respect to all the three smoothing scenarios, the smoothing condition *B/A* achieved the best desired results.

D.3 Resampling of well logs to the resolution of synthetic data

The resampling of well logs to the resolution of synthetic data in GEOVIEW is done by applying 1D data interpolation function in MATLAB. By doing this process, the original 18892 well data (6608/10-3) samples of *A* and *B* in MATLAB are now decreased to 2906 samples, i.e. to the resolution of synthetic data. The basis of doing this step is to see any effect on the estimated ⟨*Vp*⟩ and ⟨*Vp*⟩/⟨*Vs*⟩ curves due to lowering of data samples. Figure D-4 shows that no significant change is observed in both wells due to resampling.

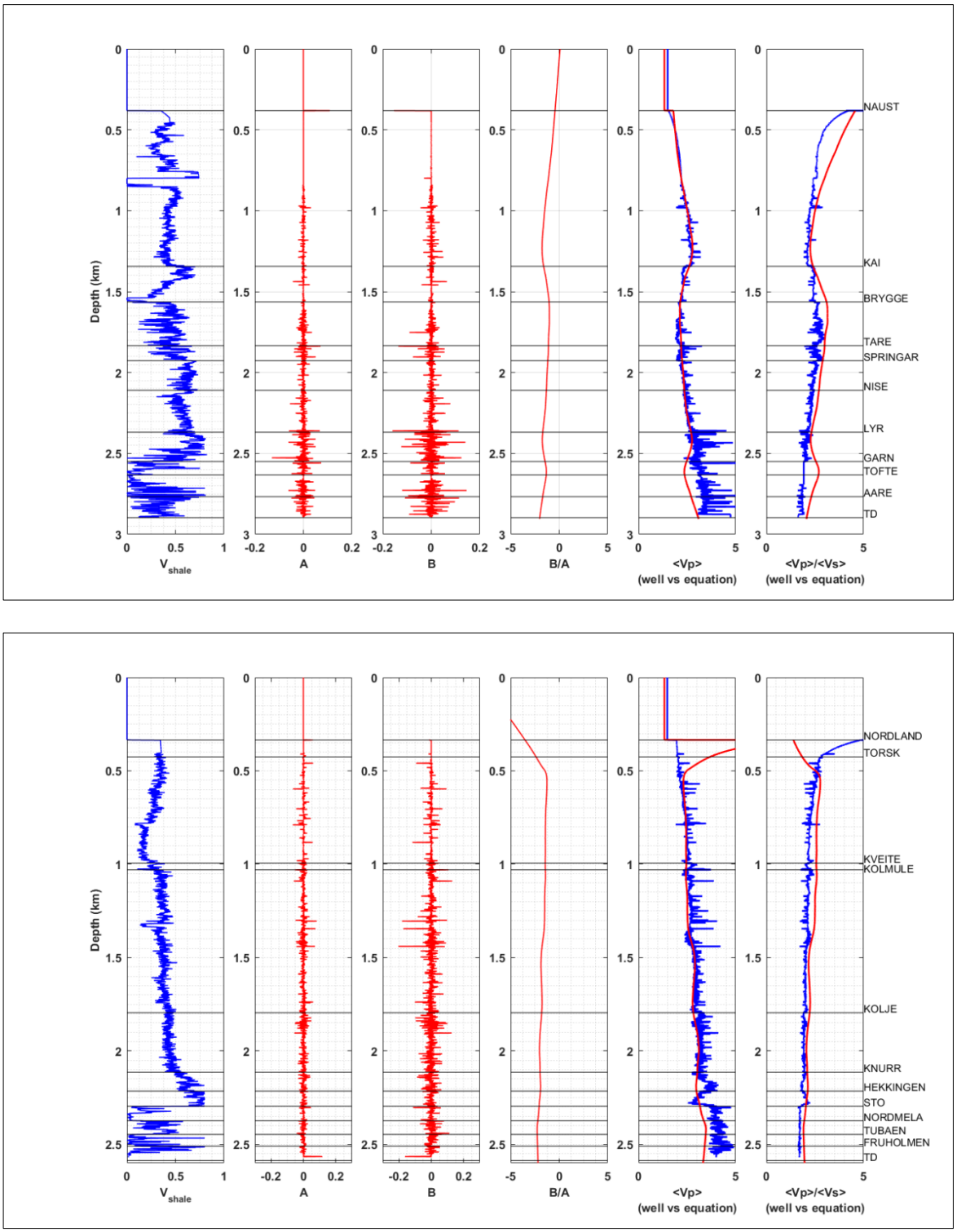

Figure D-4. ⟨*Vp*⟩ and ⟨*Vp*⟩/⟨*Vs*⟩ estimated by using data *A* and *B* to GEOVIEW resolution, smoothing *B/A* with span of 309 and constant *m*, *g* and *c* (assuming V_{sh} = 50%) for isotropic media. Well 6608/10-3, Norne Field (top) and Well 7121/4-1, Snøhvit Field (bottom).

APPENDIX E: More estimated results using seismic data

The real seismic data of Norne Field is a 2D line with CMPs at inline = 1045 and xline = 1300 – 2300. The outcome of estimated modelled curves across the whole line at different locations are shown in the following figures.

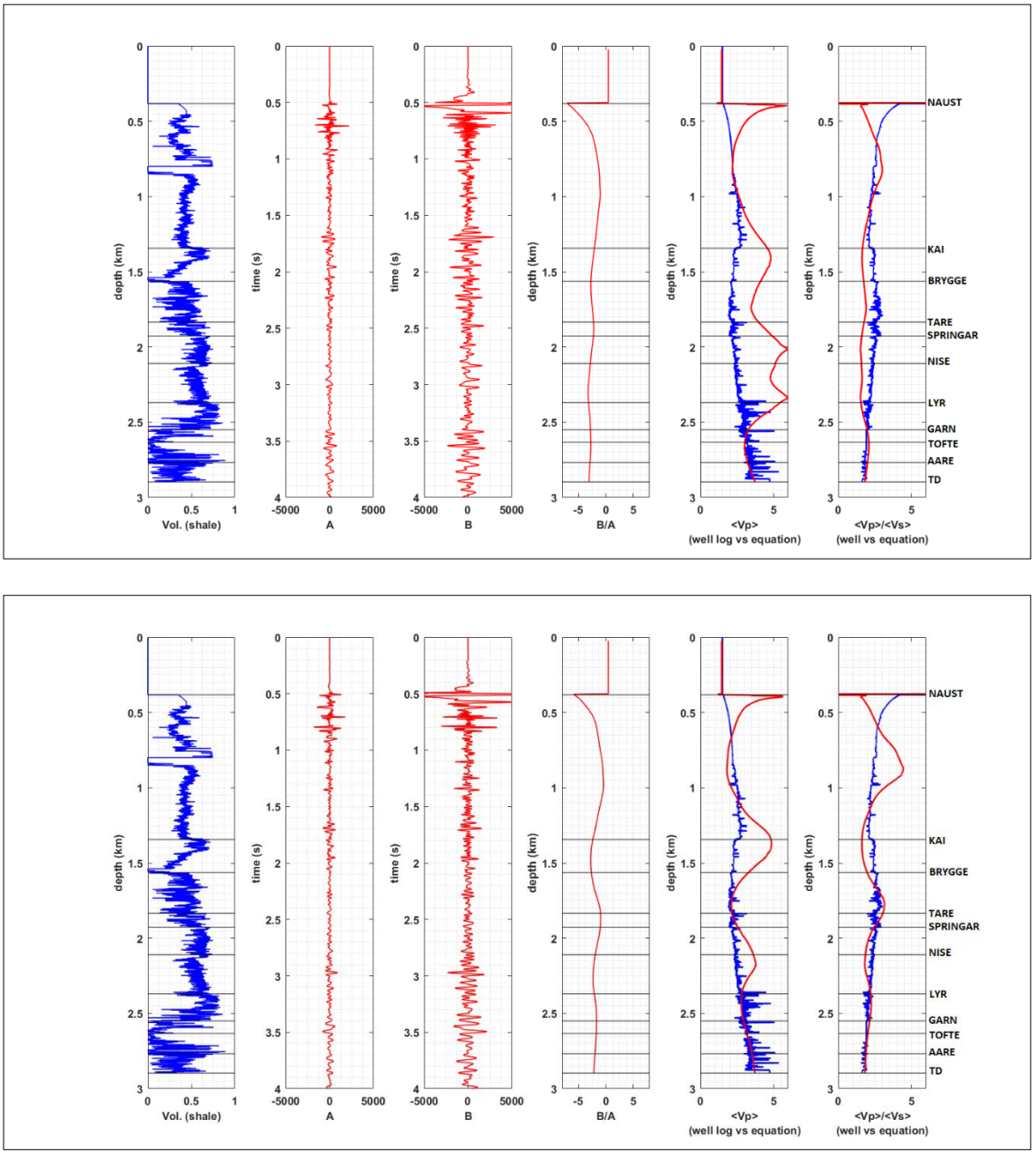

Figure E-1. ⟨*Vp*⟩/⟨*Vs*⟩ estimated by smoothing the seismic response data *B/A* and constant *m*, *g* and *c* (assuming V_{sh} = 50%) for VTI media using equation (34), Norne Field. Inline = 1045, xline = 1300 (top) and inline = 1045, xline = 1500 (bottom).

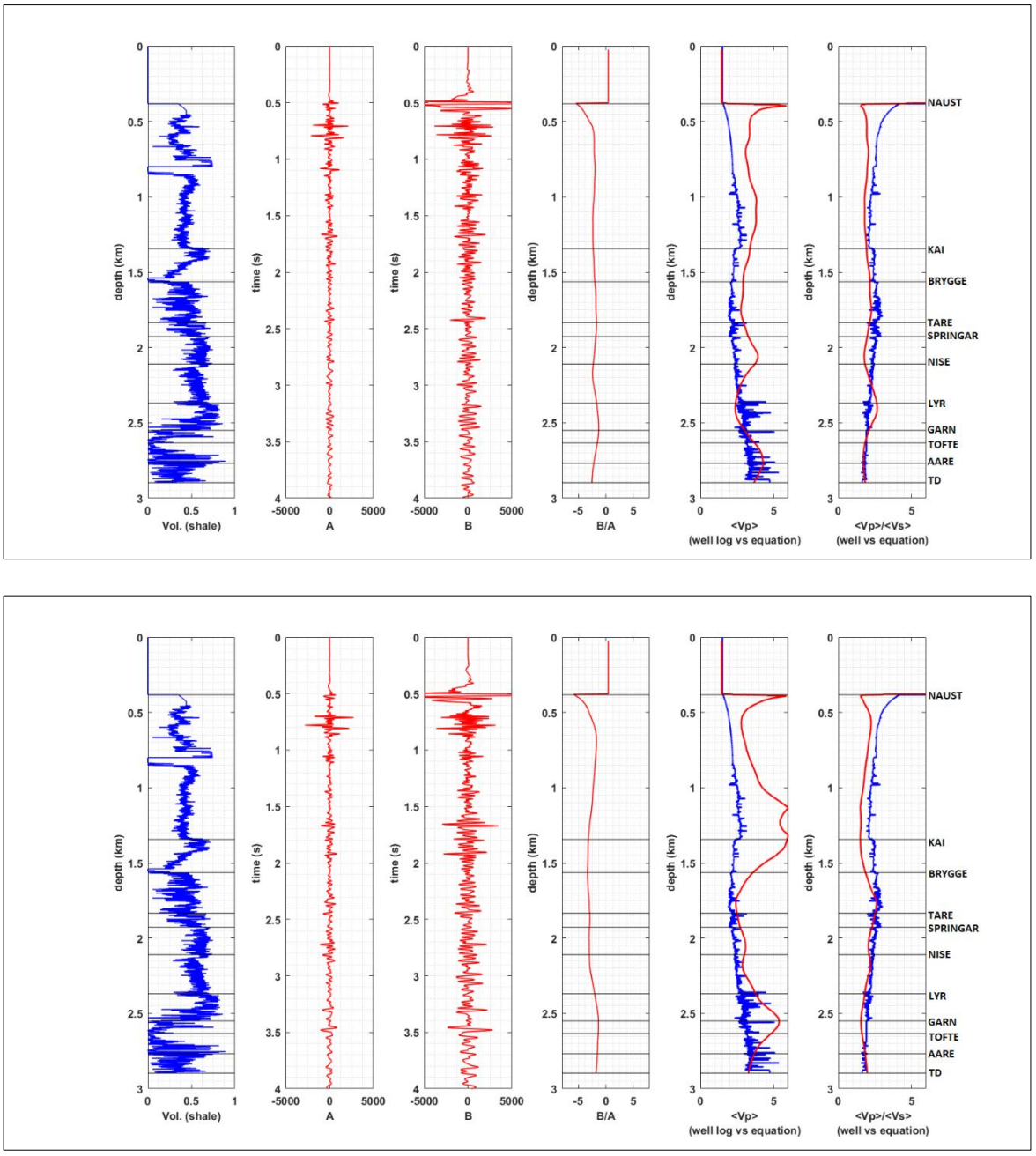

Figure E-2. ⟨*Vp*⟩/⟨*Vs*⟩ estimated by smoothing the seismic response data *B/A* and constant *m*, *g* and *c* (assuming V_{sh} = 50%) for VTI media using equation (34), Norne Field. Inline = 1045, xline = 1700 (top) and inline = 1045, xline = 1900 (bottom).

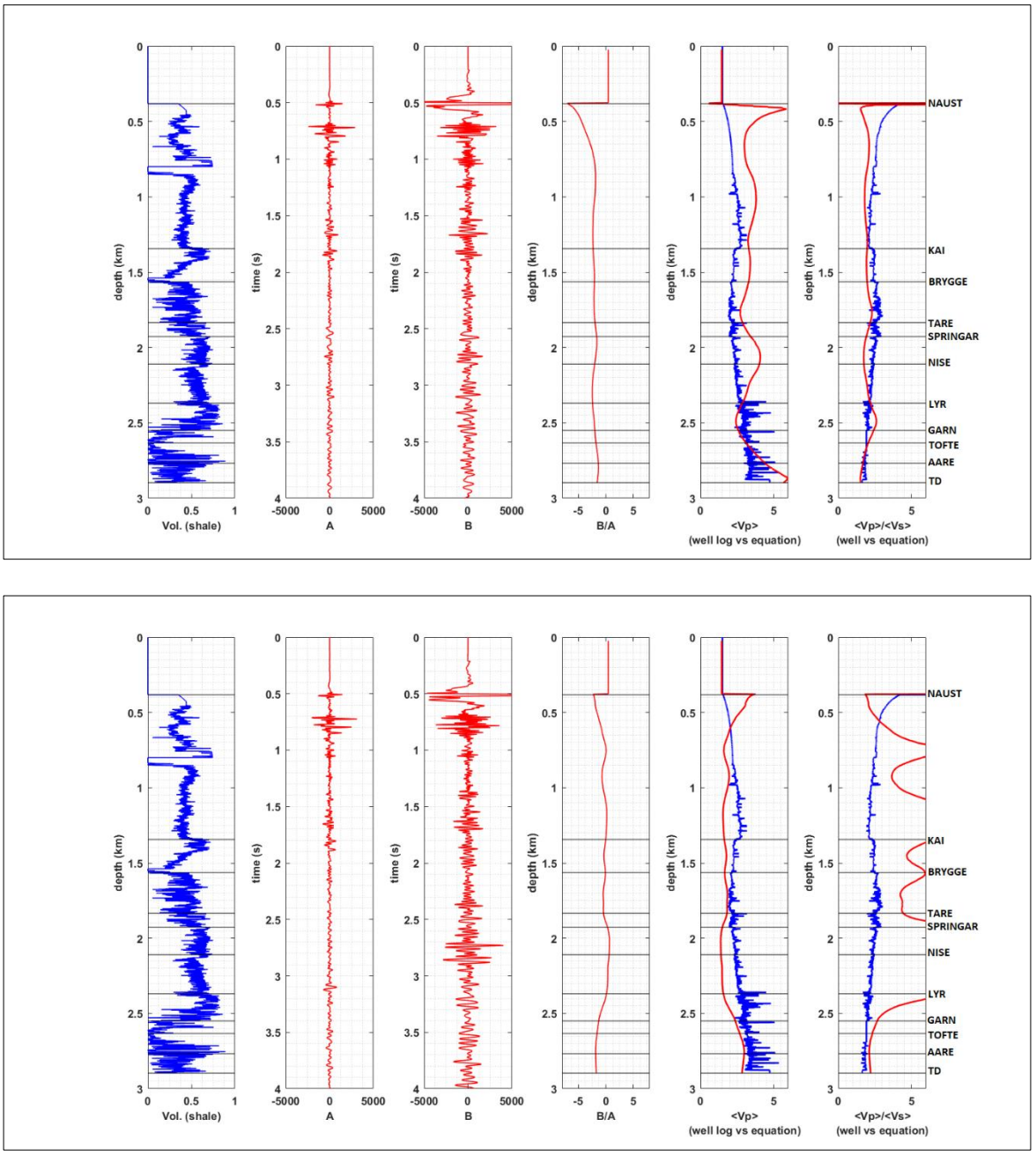

Figure E-3. ⟨*Vp*⟩/⟨*Vs*⟩ estimated by smoothing the seismic response data *B/A* and constant *m*, *g* and *c* (assuming V_{sh} = 50%) for VTI media using equation (34), Norne Field. Inline = 1045, xline = 2290 (top) and inline = 1045, xline = 2300 (bottom).

APPENDIX F: Seismic frequency bandwidth problem

The following figures show the results of estimated average *Vp* and *Vp/Vs* ratios of the well 7121/4-1, Snøhvit Field using Ricker wavelet and bandpass filter of different dominant frequencies. As seen from the various output, it clearly shows that the separation, fluctuations between the modelled curves and the well log data curves get reduced with increase of frequency.

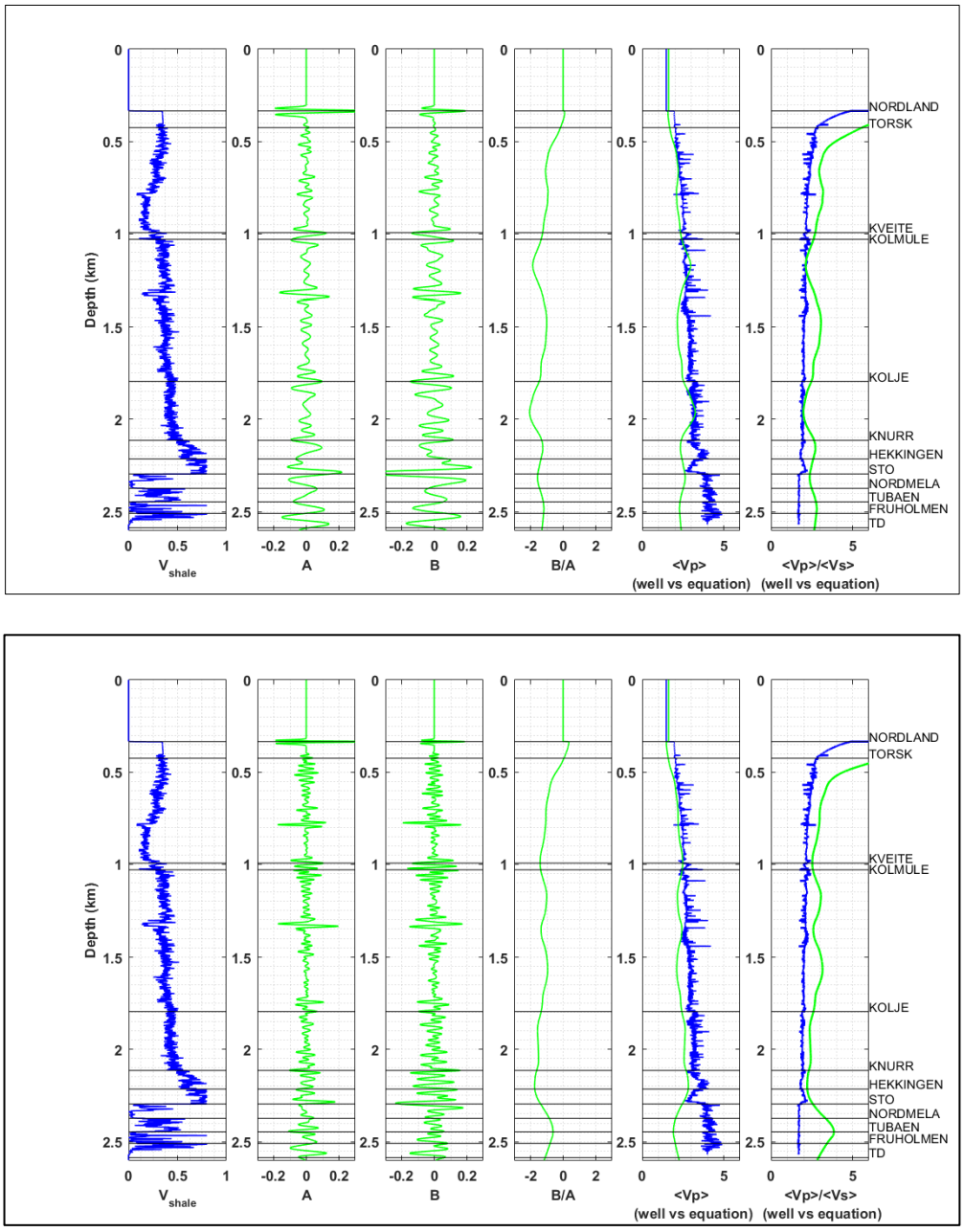

Figure F-1. ⟨*Vp*⟩/⟨*Vs*⟩ estimated by smoothing the response data *B/A* using Ricker wavelet of 20 Hz (top) and 40 Hz (bottom) frequency for VTI media, equation (34). Well 7121/4-1, Snøhvit Field.

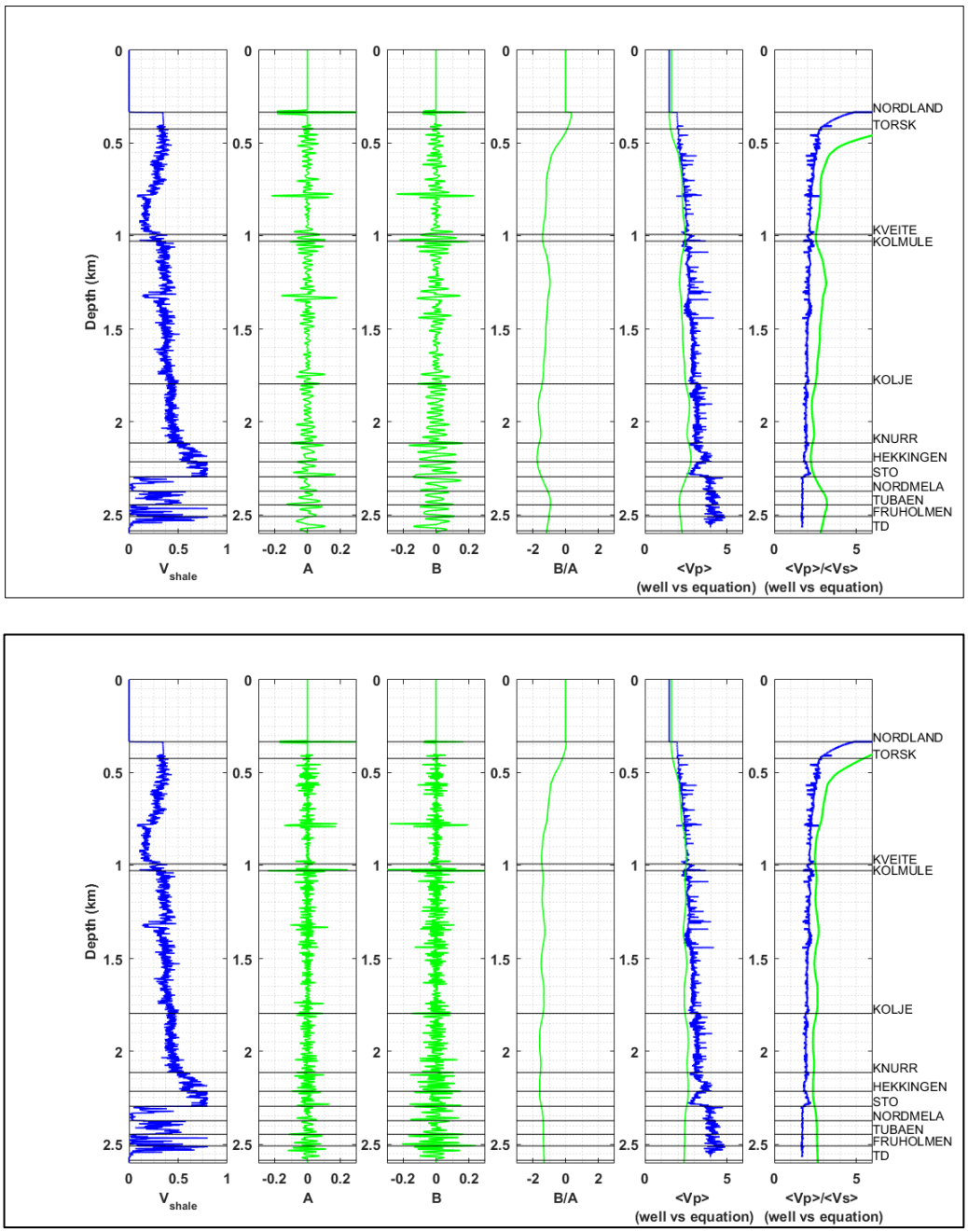

Figure F-2. ⟨*Vp*⟩/⟨*Vs*⟩ estimated by smoothing the response data *B/A* using Ricker wavelet of 50 Hz (top) and 100 Hz (bottom) frequency for VTI media, equation (34). Well 7121/4-1, Snøhvit Field.

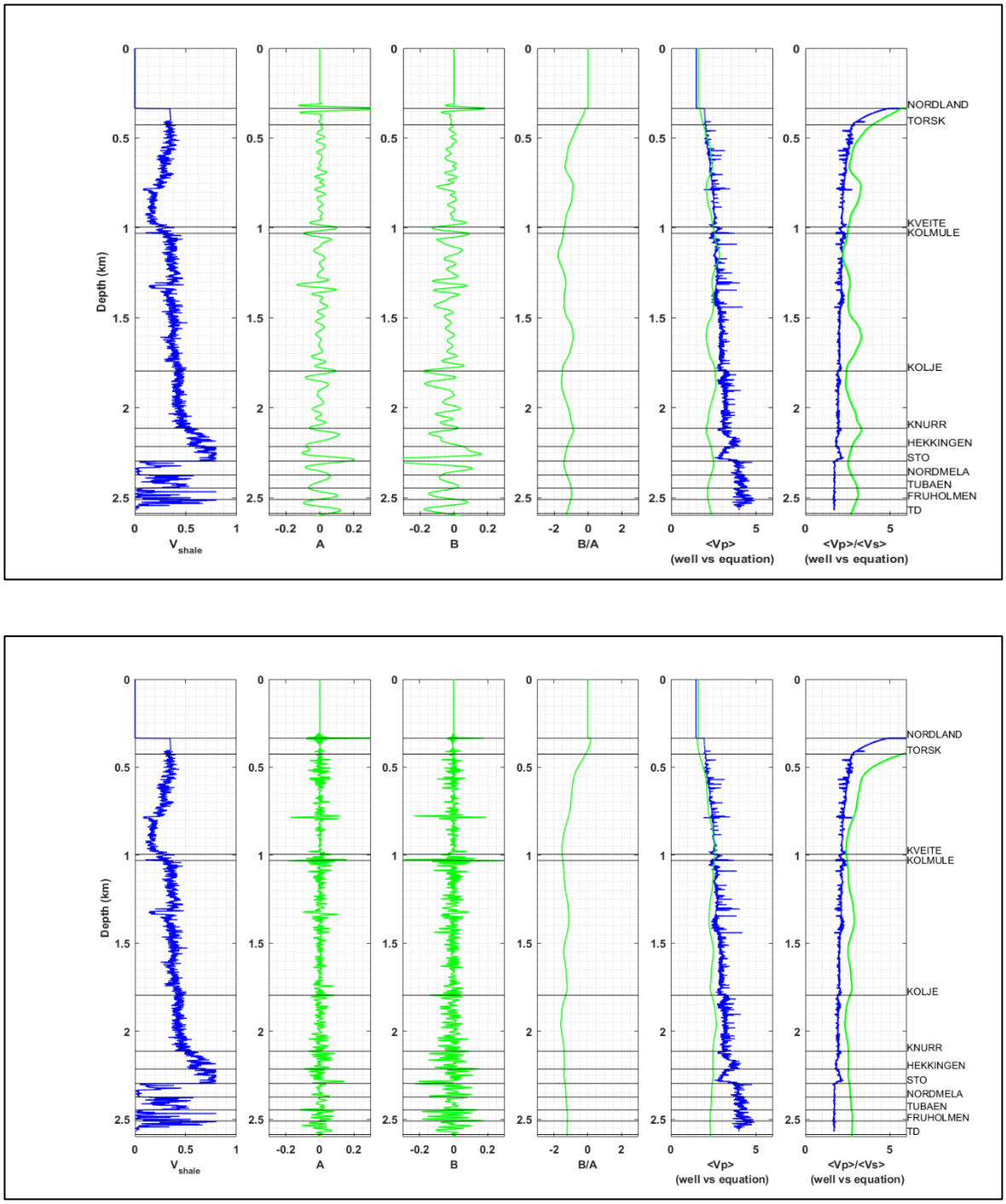

Figure F-3. ⟨*Vp*⟩/⟨*Vs*⟩ estimated by smoothing the response data *B/A* using bandpass wavelet, frequencies of 1, 5, 30 and 40 Hz (top) and 1, 5, 150 and 160 Hz (bottom) for VTI media, equation (34). Well 7121/4-1, Snøhvit Field.